

Electronic Supplementary Information (ESI)

Ligand Properties of Boryl Ligands in bis-Boryl Rhodium(III) Complexes: A Case Study

Wiebke Drescher[†] and Christian Kleeberg^{†,*}

[†]Institut für Anorganische und Analytische Chemie, Technische Universität Braunschweig, Germany.

* Author E-mail Address: ch.kleeberg@tu-braunschweig.de

Contents

1. Experimental and Spectroscopic Data	
a. Additional Experimental Data	
[Rh(PPh ₃) ₂ (Bcat)(Bpin)Cl]	S2
b. <i>In situ</i> NMR experiments:	
Reaction of [Rh(PMe ₃) ₃ Cl] with the diboranes(4) 1a–e	S3
[Rh(PMe ₃) ₃ (Bpin) ₂ Cl] (2b) + PMe ₃	S11
c. VT-NMR spectra of 2a–c , 3b :	
[Rh(PMe ₃) ₃ (Bcat) ₂ Cl] (2a)	S12
[Rh(PMe ₃) ₃ (Bpin) ₂ Cl] (2b)	S13
[Rh(PMe ₃) ₂ (Bpin) ₂ Cl] (3b)	S14
[Rh(PMe ₃) ₃ (Bpin) ₂ Cl] · [Rh(PMe ₃) ₂ (Bpin) ₂ Cl] (2b · 3b)	S15
[Rh(PMe ₃) ₃ (Bcat)(Bpin)Cl] (2c)	S17
d. VT-NMR spectra of 4a–c , 5c , 6c :	
[Rh(PMe ₃) ₄ (Bcat) ₂][BArF] (4a)	S18
[Rh(PMe ₃) ₄ (Bpin) ₂][BArF] (4b)	S19
[Rh(PMe ₃) ₄ (Bcat)(Bpin)] [BArF] (4c)	S20
[[Rh(PMe ₃) ₃ (NCMe)(Bcat)(Bpin)] [BArF] (5c)	S21
[Rh(PMe ₃) ₃ (CNMe)(Bcat)(Bpin)] [BArF] (6c)	S22
2. Crystallographic Data	
a. Crystallographic Data Collection Parameters	S23
b. [(Me ₃ P) ₄ RhH(Cl)][B(1,2-O ₂ C ₆ H ₄) ₂](THF)	S27
c. [(Me ₃ P) ₂ Rh(Bpin) ₂ (Cl)] (3b) and 2b · 3b	S28
d. [Rh(PPh ₃) ₂ (Bcat)(Bpin)(Cl)](CH ₂ Cl ₂) _{3.5} (C ₅ H ₁₂) _{0.6}	S30
e. [Rh(PMe ₃) ₃ (Bcat)(Bpin)(L)][BArF] (L = MeCN (5c), MeNC (6c))	S31
3. References	S32

1. Experimental and Spectroscopic Data

1.a. Additional Experimental Data

[Rh(PPh₃)₂(Bcat)(Bpin)(Cl)]

[Rh(PPh₃)₃Cl] (30 mg, 32 µmol, 1 eq.) and pinB-Bcat (**1c**) (8 mg, 32 mmol, 1 eq.) were dissolved in DCM/*n*-pentane (17 mL, 1:1). After 16 at rt all volatiles were removed *in vacuo* and the residue dissolved in DCM (0.5 mL) and layered with *n*-pentane (2 mL). After several days a few single crystals suitable for x-ray analysis of the approximate composition [Rh(PPh₃)₂(Bcat)(Bpin)(Cl)](CH₂Cl₂)_{3.5}(C₅H₁₂)_{0.5} had separated.

1.b. *In situ* NMR experiments: Reaction of [Rh(PMe₃)₃Cl] with the diboranes(4) 1a-e

General Procedure: To a solution of [Rh(PMe₃)₃Cl] (15 mg, 41 μmol, 1.0 eq.) in C₆D₆ or THF-d₈ (0.7 mL) an equimolar amount of the diborane(4) derivative (41 μmol, 1.0 equiv.) was added and the solution transferred to a screw-cap NMR Tube. The NMR spectra were recorded in the given intervals.

[Rh(PMe₃)₃Cl] with 1a

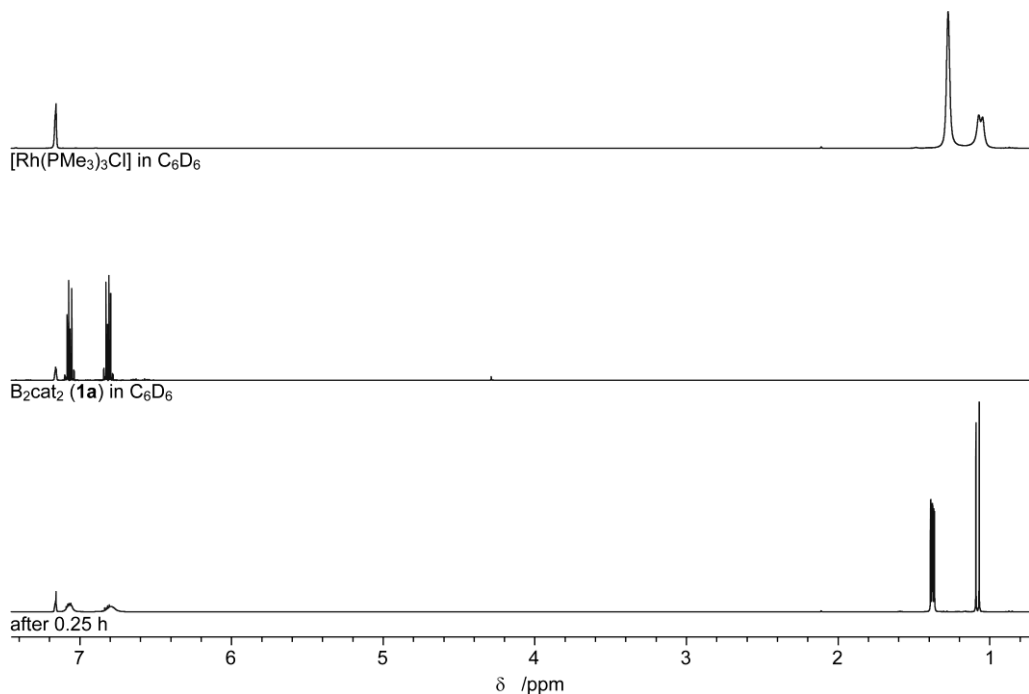


Figure S1b.1: *In situ* ¹H NMR spectra of the reaction of [Rh(PMe₃)₃Cl] with **1a** and spectra of **1a** and [Rh(PMe₃)₃Cl] for comparison (300.3 MHz, C₆D₆, rt).

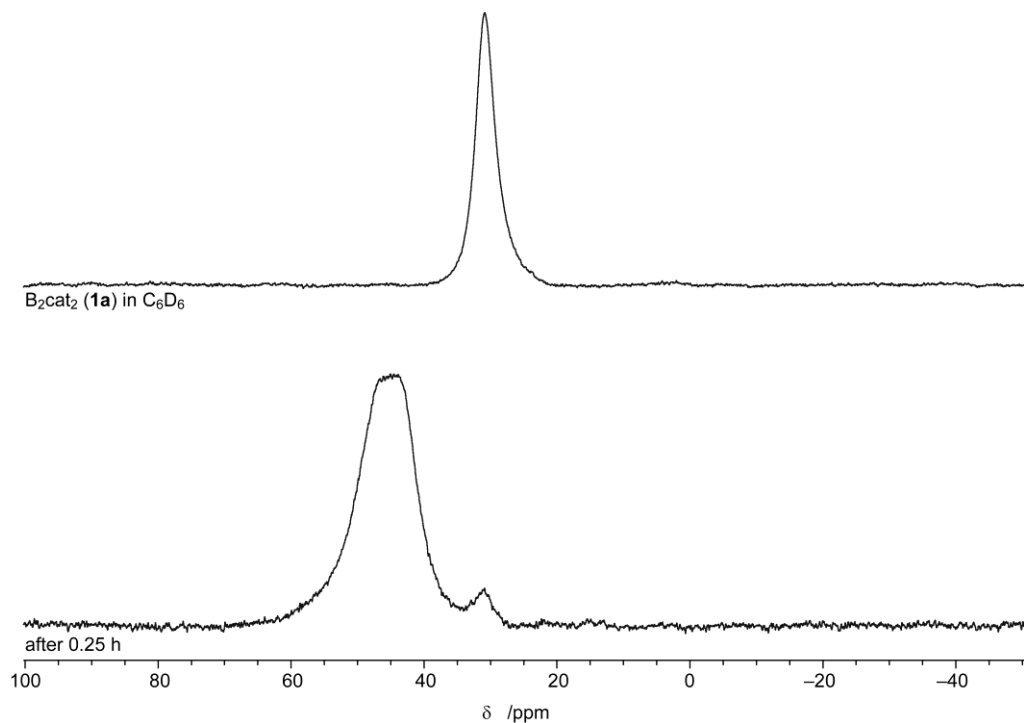


Figure S1b.2: *In situ* $^{11}\text{B}\{^1\text{H}\}$ NMR spectra of the reaction of $[\text{Rh}(\text{PMe}_3)_3\text{Cl}]$ with **1a** and a spectrum of **1a** for comparison (96.3 MHz, C_6D_6 , rt).

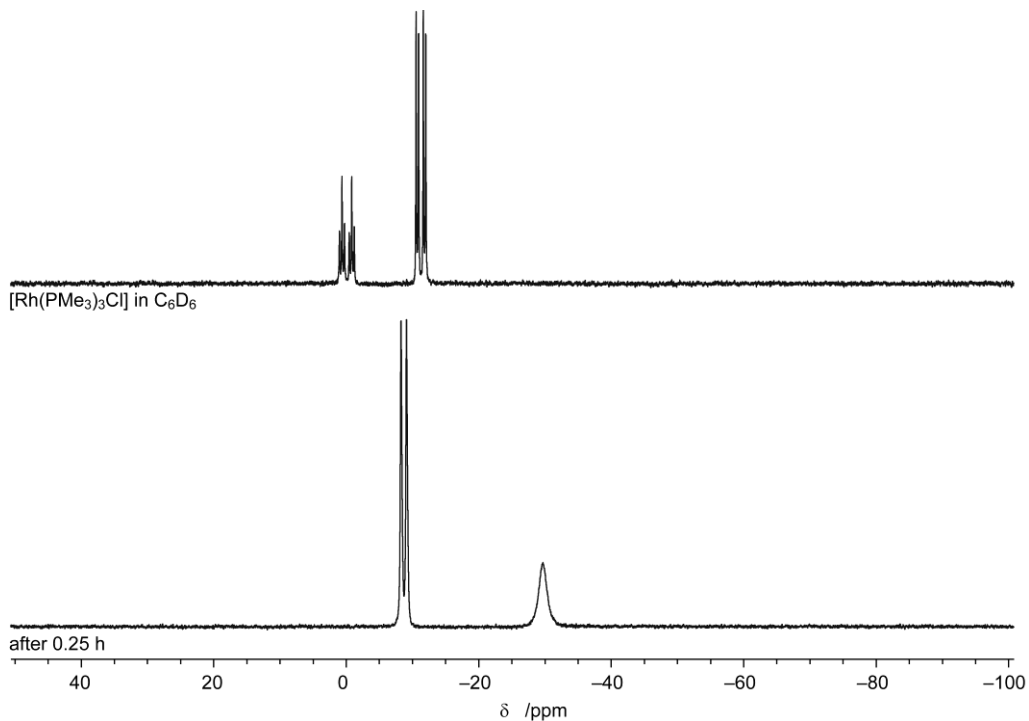


Figure S1b.3: *In situ* $^{31}\text{P}\{^1\text{H}\}$ NMR spectra of the reaction of $[\text{Rh}(\text{PMe}_3)_3\text{Cl}]$ with **1a** and a spectrum of $[\text{Rh}(\text{PMe}_3)_3\text{Cl}]$ for comparison (121.5 MHz, C_6D_6 , rt).

[Rh(PMe₃)₃Cl] with 1b

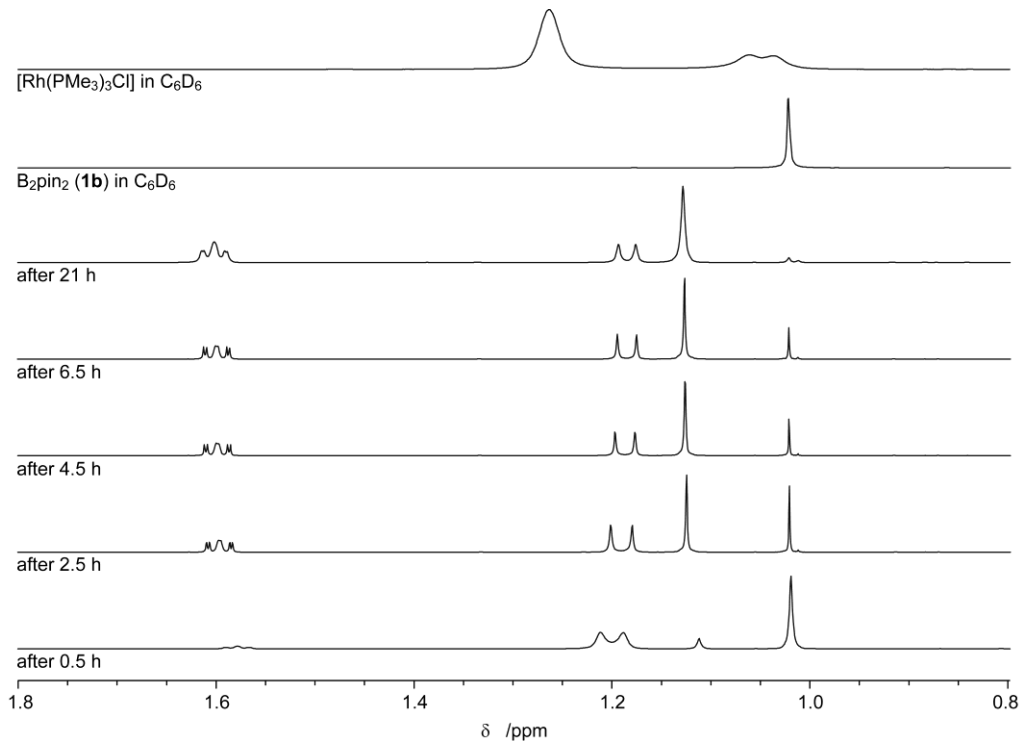


Figure S1b.4: *In situ* ¹H NMR spectra of the reaction of [Rh(PMe₃)₃Cl] with **1b** and spectra of **1b** and [Rh(PMe₃)₃Cl] for comparison (300.3 MHz, C₆D₆, rt).

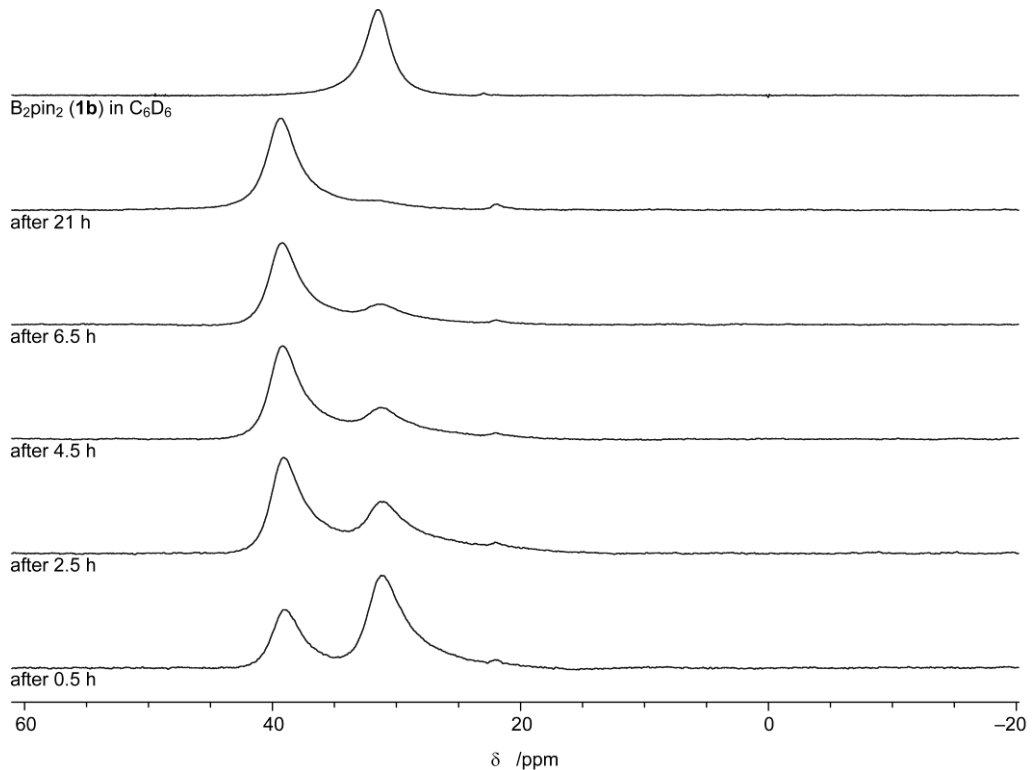


Figure S1b.5: *In situ* ¹¹B(¹H) NMR spectra of the reaction of [Rh(PMe₃)₃Cl] with **1b** and a spectrum of **1b** for comparison (96.3MHz, C₆D₆, rt).

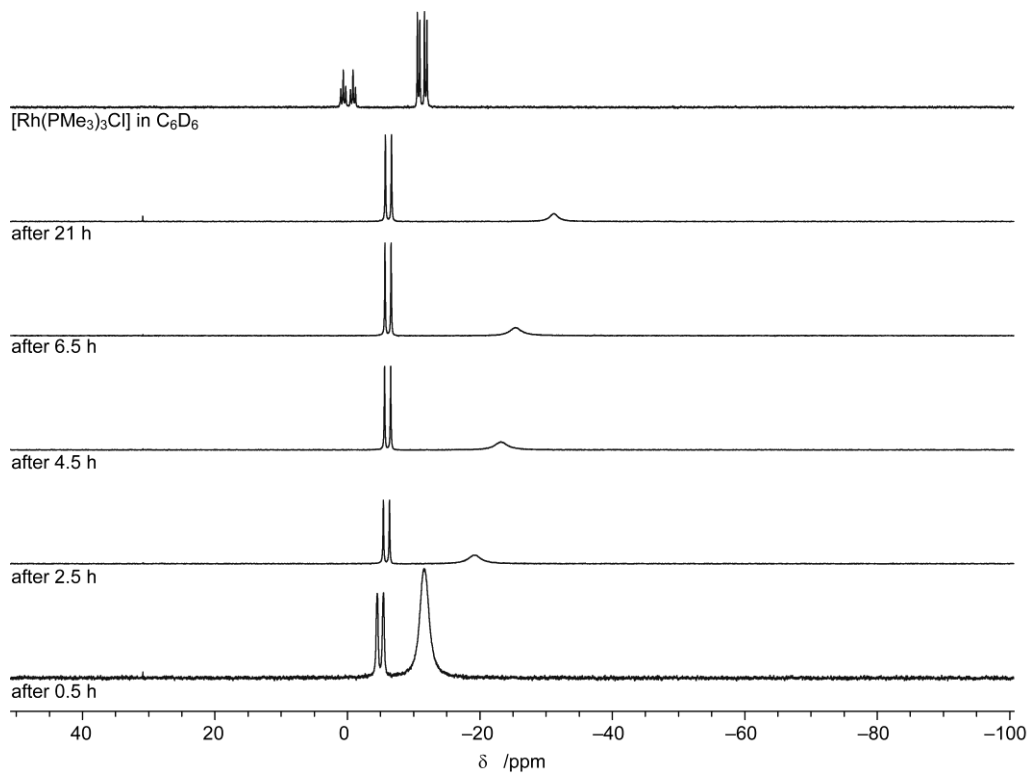


Figure S1b.6: *In situ* $^{31}\text{P}\{\text{H}\}$ NMR spectra of the reaction of [Rh(PMe₃)₃Cl] with **1b** and a spectrum of [Rh(PMe₃)₃Cl] for comparison (121.5 MHz, C₆D₆, rt).

[Rh(PMe₃)₃Cl] with **1c**

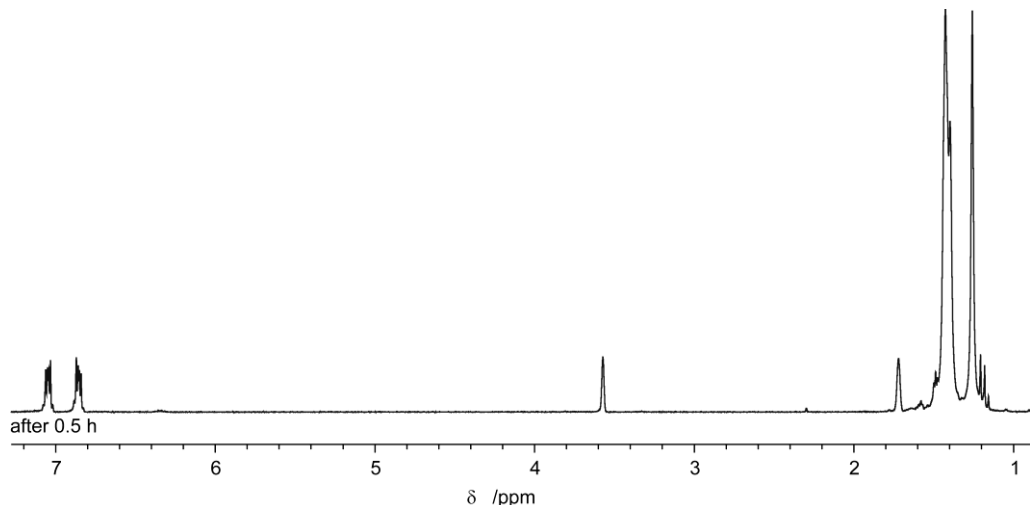


Figure S1b.7: *In situ* ^1H NMR spectra of the reaction of [Rh(PMe₃)₃Cl] with **1c** (300.3 MHz, THF-d₈, rt).

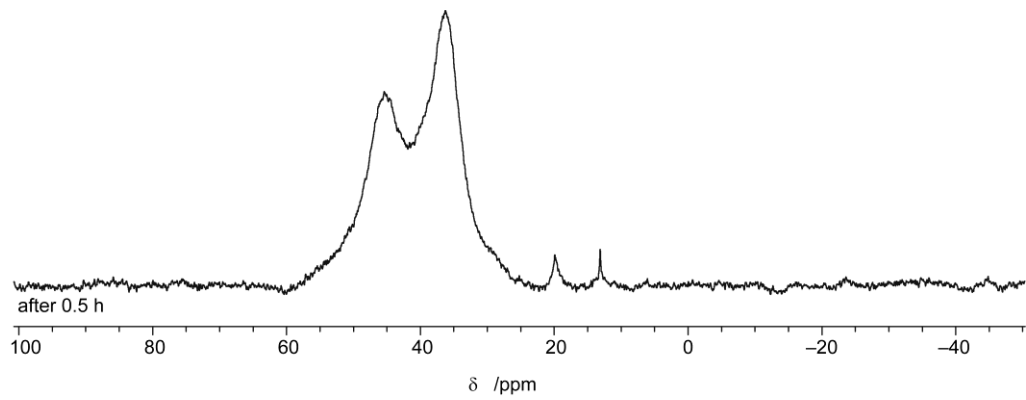


Figure S1b.8: *In situ* $^{11}\text{B}\{\text{H}\}$ NMR spectra of the reaction of $[\text{Rh}(\text{PMe}_3)_3\text{Cl}]$ with **1c** (96.3 MHz, THF-d₈, rt).

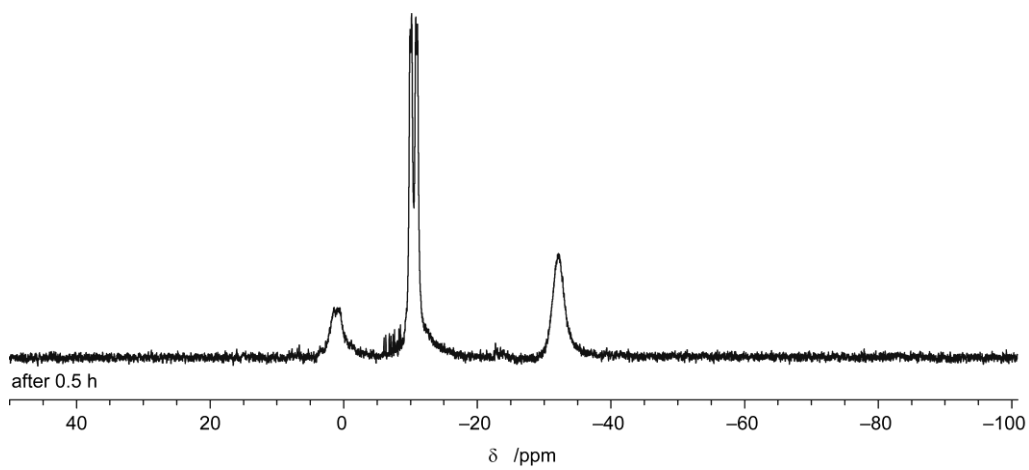


Figure S1b.9: *In situ* $^{31}\text{P}\{\text{H}\}$ NMR spectra of the reaction of $[\text{Rh}(\text{PMe}_3)_3\text{Cl}]$ with **1c** (121.5 MHz, THF-d₈, rt).

[Rh(PMe₃)₃Cl] with **1d**

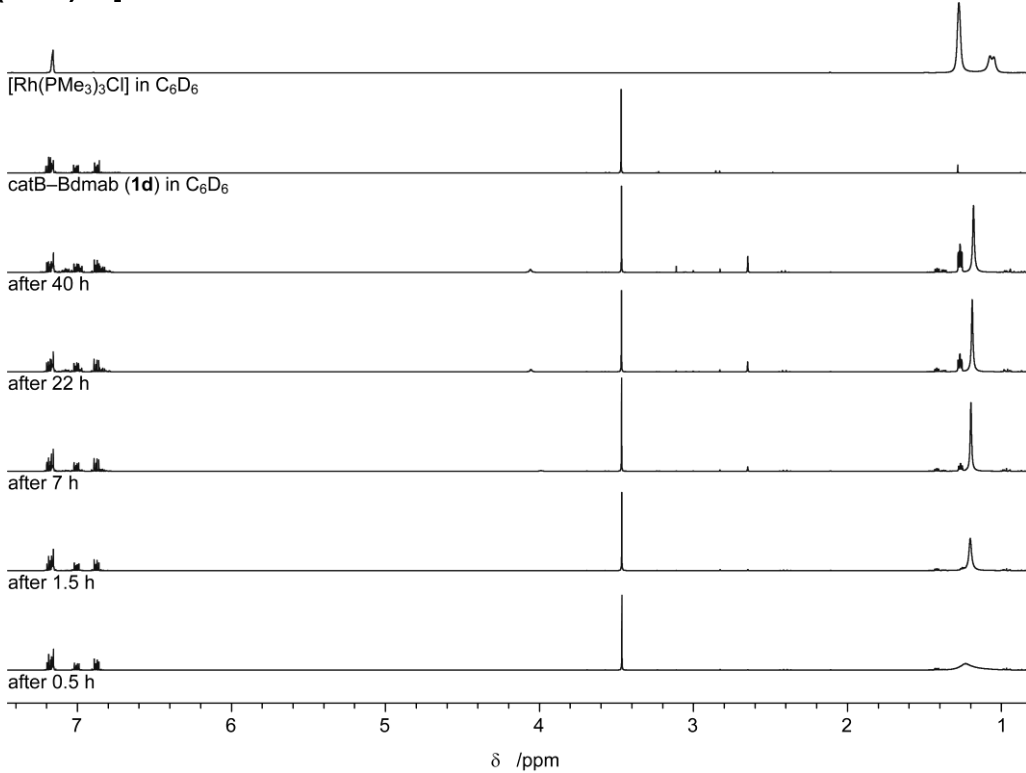


Figure S1b.10: *In situ* ¹H NMR spectra of the reaction of [Rh(PMe₃)₃Cl] with **1d** and spectra of **1d** and [Rh(PMe₃)₃Cl] for comparison (300.3 MHz, C₆D₆, rt).

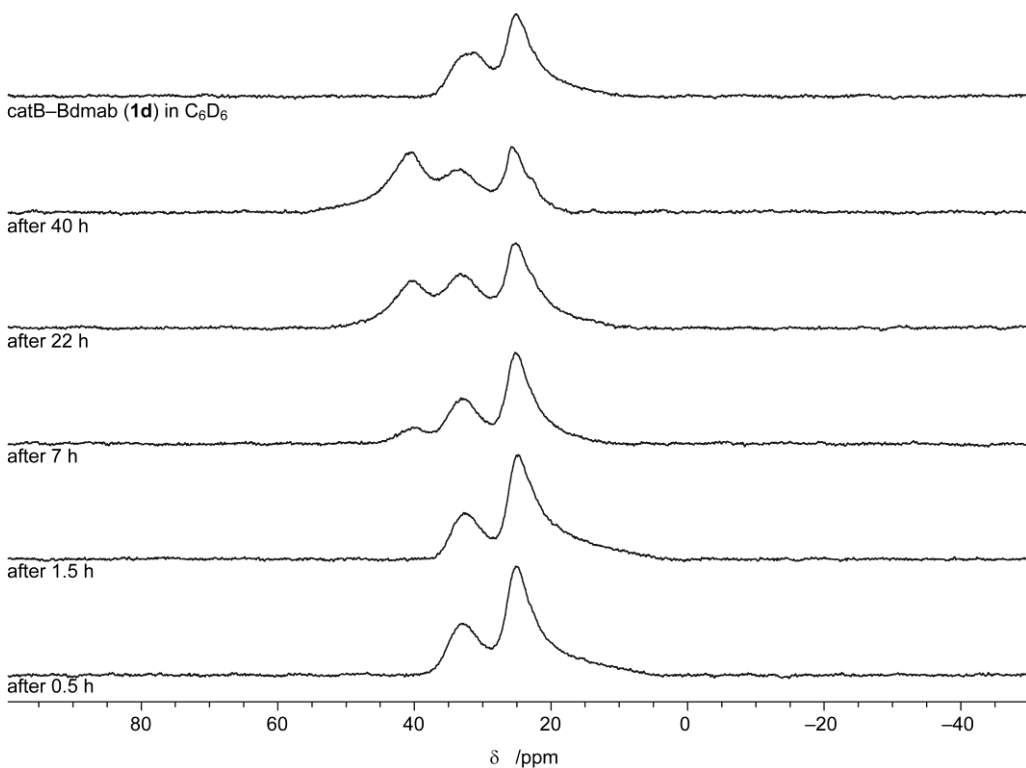


Figure S1b.11: *In situ* ¹¹B{¹H} NMR spectra of the reaction of [Rh(PMe₃)₃Cl] with **1d** and a spectrum of **1d** for comparison (96.3 MHz, C₆D₆, rt).

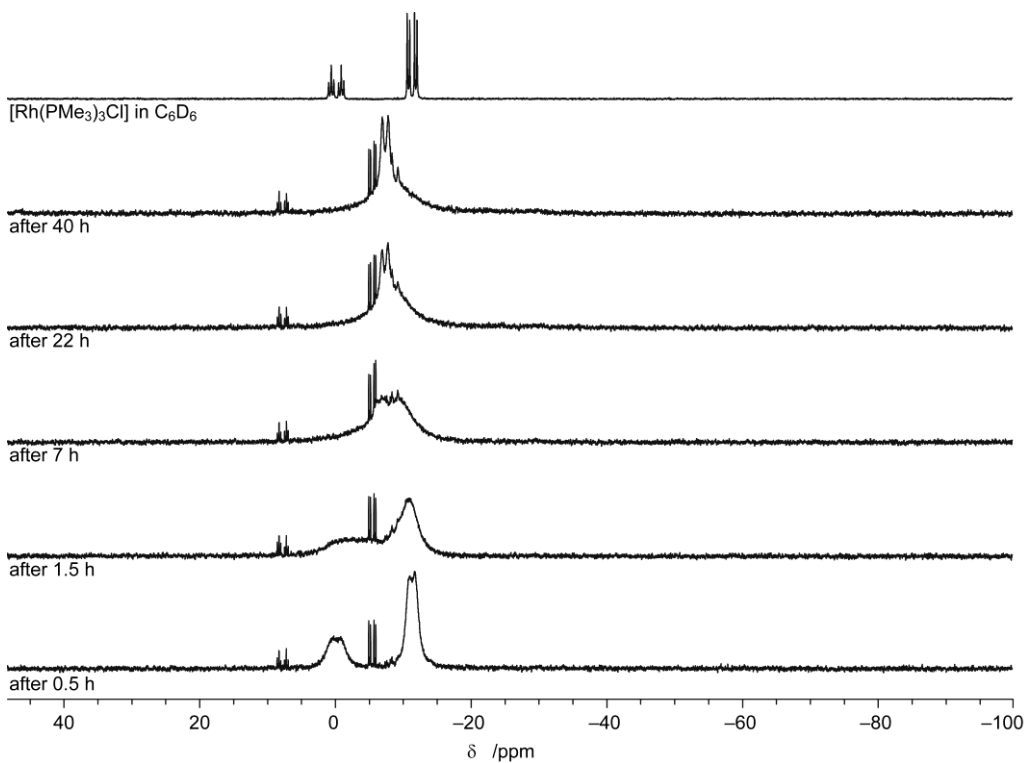


Figure S1b.12: *In situ* $^{31}\text{P}\{\text{H}\}$ NMR spectra of the reaction of $[\text{Rh}(\text{PMe}_3)_3\text{Cl}]$ with **1d** and a spectrum of $[\text{Rh}(\text{PMe}_3)_3\text{Cl}]$ for comparison (121.5 MHz, C_6D_6 , rt).

$[\text{Rh}(\text{PMe}_3)_3\text{Cl}]$ with **1e**

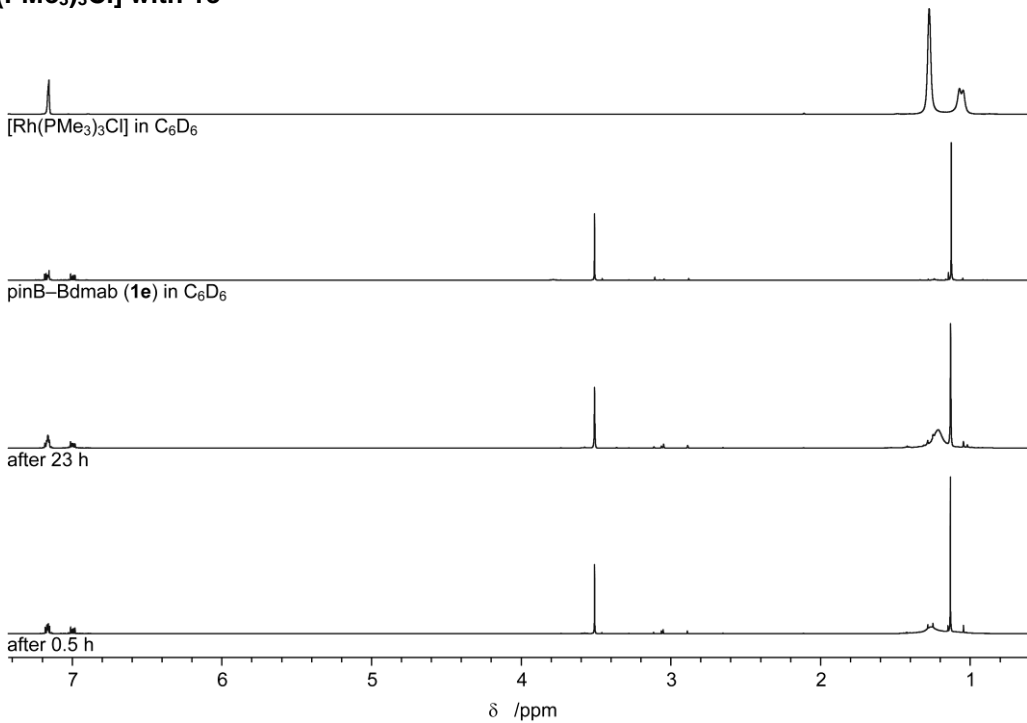


Figure S1b.13: *In situ* ^1H NMR spectra of the reaction of $[\text{Rh}(\text{PMe}_3)_3\text{Cl}]$ with **1e** and spectra of **1e** and $[\text{Rh}(\text{PMe}_3)_3\text{Cl}]$ for comparison (300.3 MHz, C_6D_6 , rt).

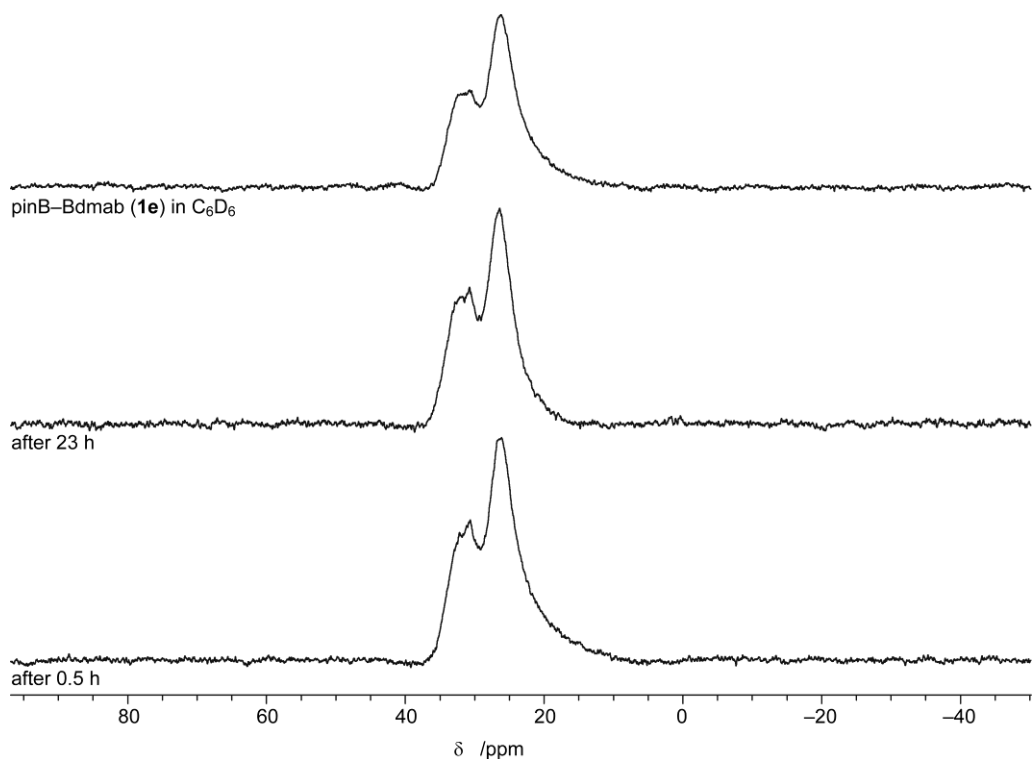


Figure S1b.14: *In situ* $^{11}\text{B}\{\text{H}\}$ NMR spectra of the reaction of $[\text{Rh}(\text{PMe}_3)_3\text{Cl}]$ with **1e** and a spectrum of **1e** for comparison (96.3 MHz, C_6D_6 , rt).

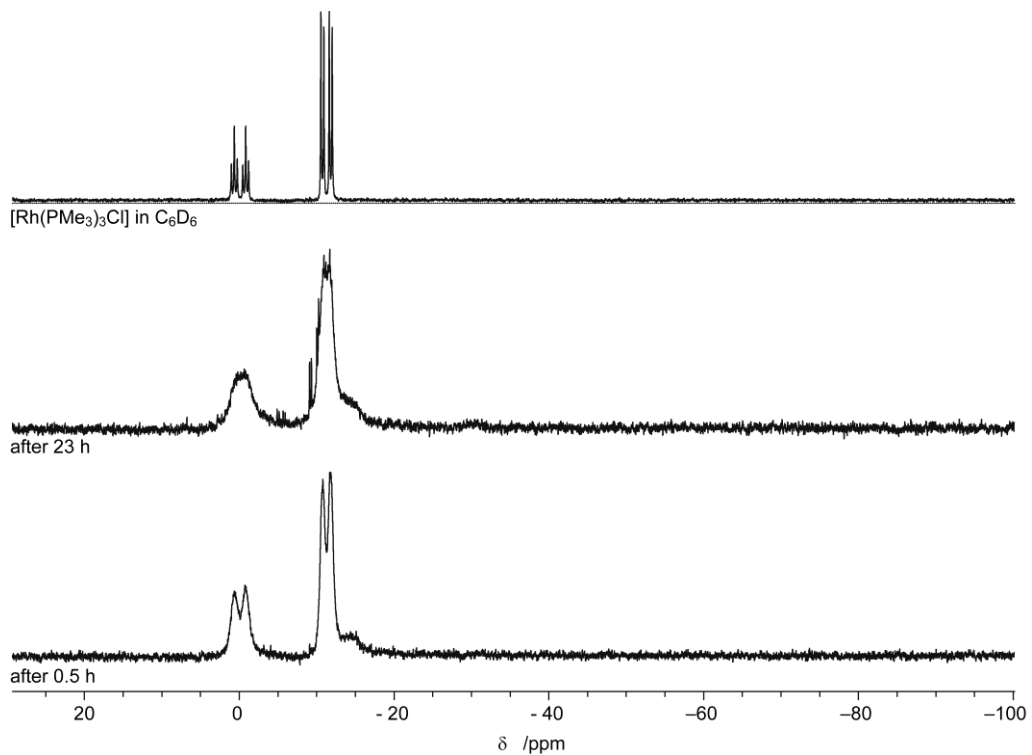


Figure S1b.15: *In situ* $^{31}\text{P}\{\text{H}\}$ NMR spectra of the reaction of $[\text{Rh}(\text{PMe}_3)_3\text{Cl}]$ with **1e** and a spectrum of $[\text{Rh}(\text{PMe}_3)_3\text{Cl}]$ for comparison (121.5 MHz, C_6D_6 , rt).

[Rh(PMe₃)₃(Bpin)₂Cl] (2b) + PMe₃

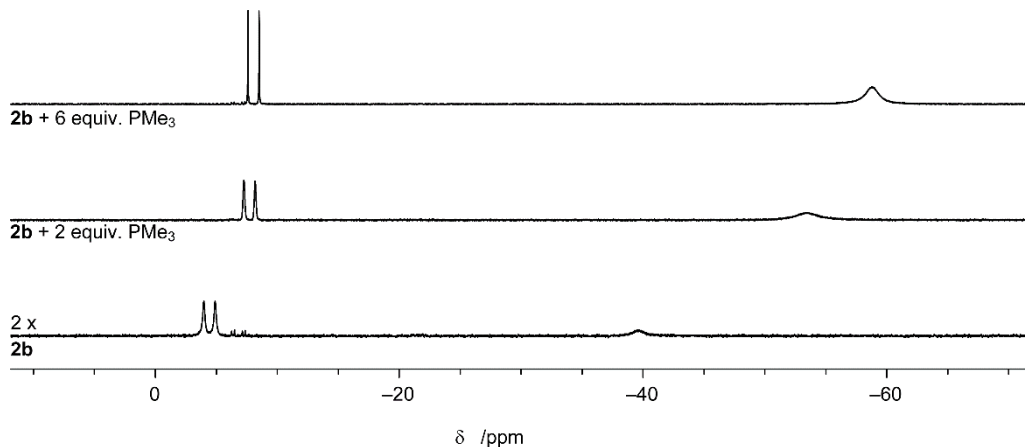


Figure S1b.16: $^{31}\text{P}\{^1\text{H}\}$ NMR spectra of $[\text{Rh}(\text{PMe}_3)_3(\text{Bpin})_2\text{Cl}]$ (**2b**) with different amounts of PMe_3 added (121.5 MHz, C_6D_6 , rt).

The observed chemical shifts of 53.5 ppm with 2 equiv. PMe_3 and 58.8 ppm with 6 equiv. PMe_3 added are well described by the weighted averaged chemical shifts of the *trans*-B PMe_3 ligand in **2b**, ($\delta_{2\mathbf{b}} = -37.9$ ppm in C_6D_6) and the chemical shift of free PMe_3 ($\delta_{\text{PMe}_3} = -62$ ppm):

$$\delta_{av} = \frac{\delta_{2\mathbf{b}} + \delta_{\text{PMe}_3}}{n_{2\mathbf{b}} + n_{\text{PMe}_3}}$$

Resulting in: $\delta_{av} = 54.0$ ppm for 2 equiv. PMe_3
 $\delta_{av} = 58.6$ ppm for 6 equiv. PMe_3

1.c. VT-NMR spectra of 2a–c, 3b

[Rh(PMe₃)₃(Bcat)₂Cl] (2a)

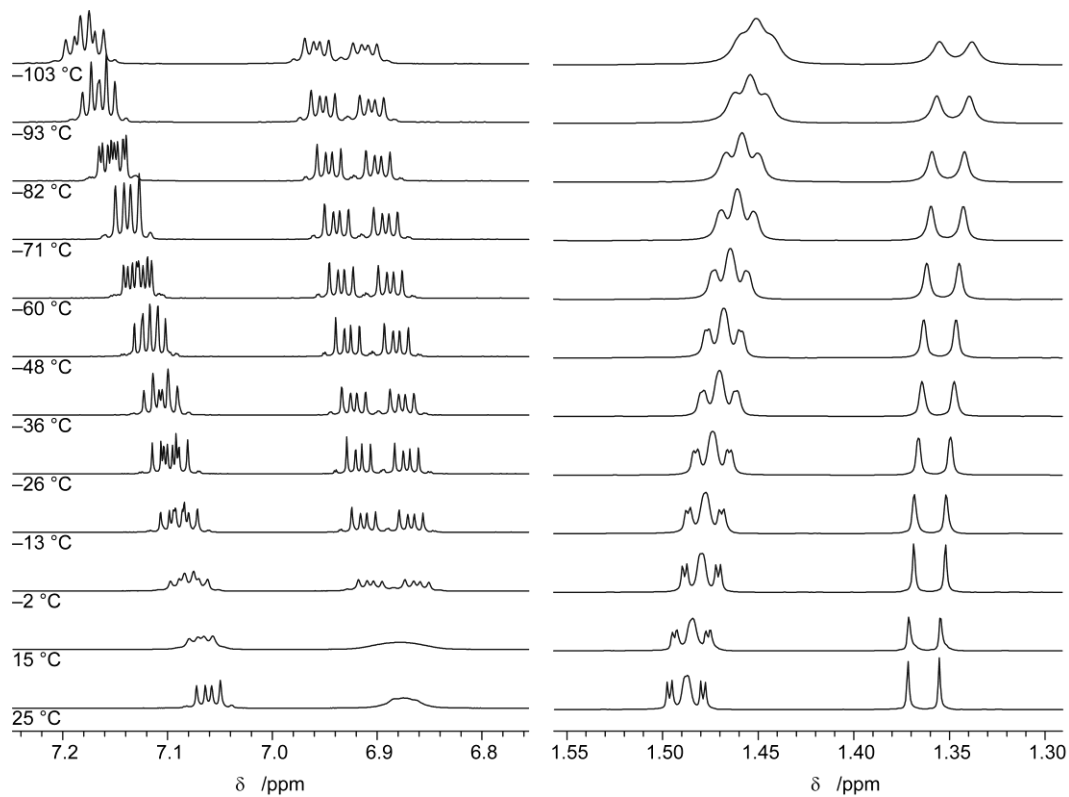


Figure S1c.1: VT-¹H NMR spectra of **2a** (400.4 MHz, THF-d₈).

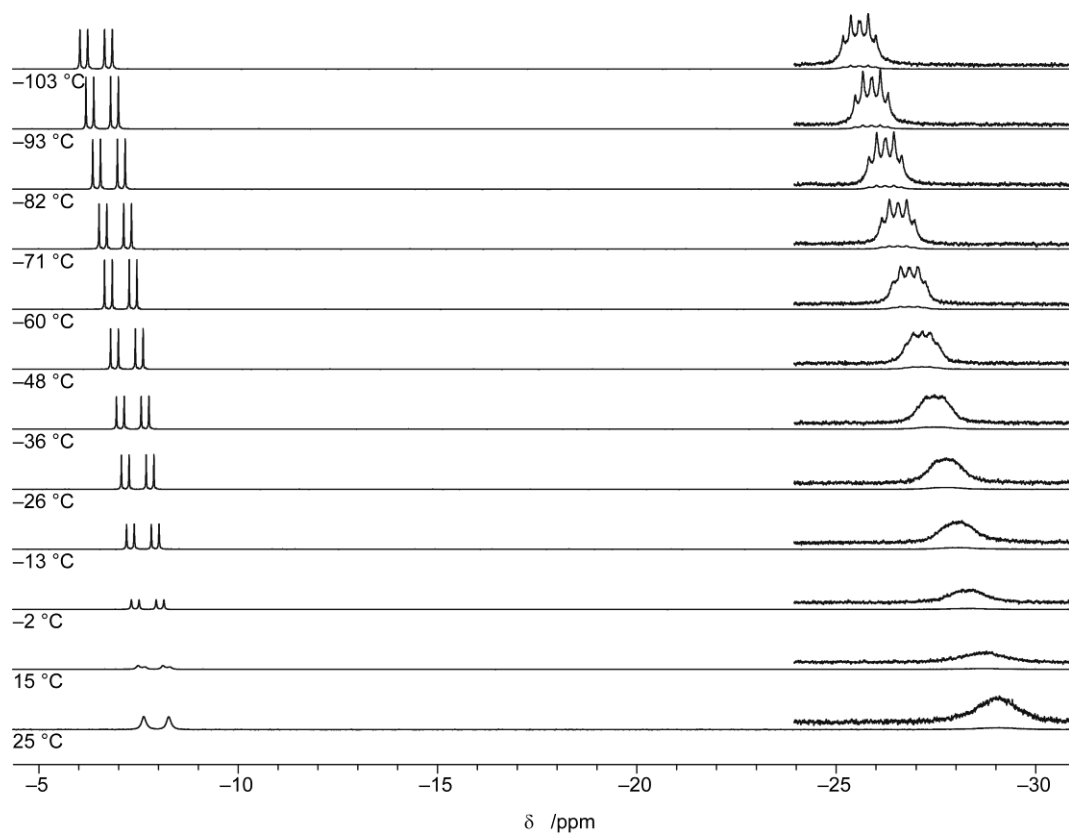


Figure S1c.2: VT-³¹P{¹H} NMR spectra of **2a** (inset: $\times 10$) (162.1 MHz, THF-d₈).

[Rh(PMe₃)₃(Bpin)₂Cl] (2b)

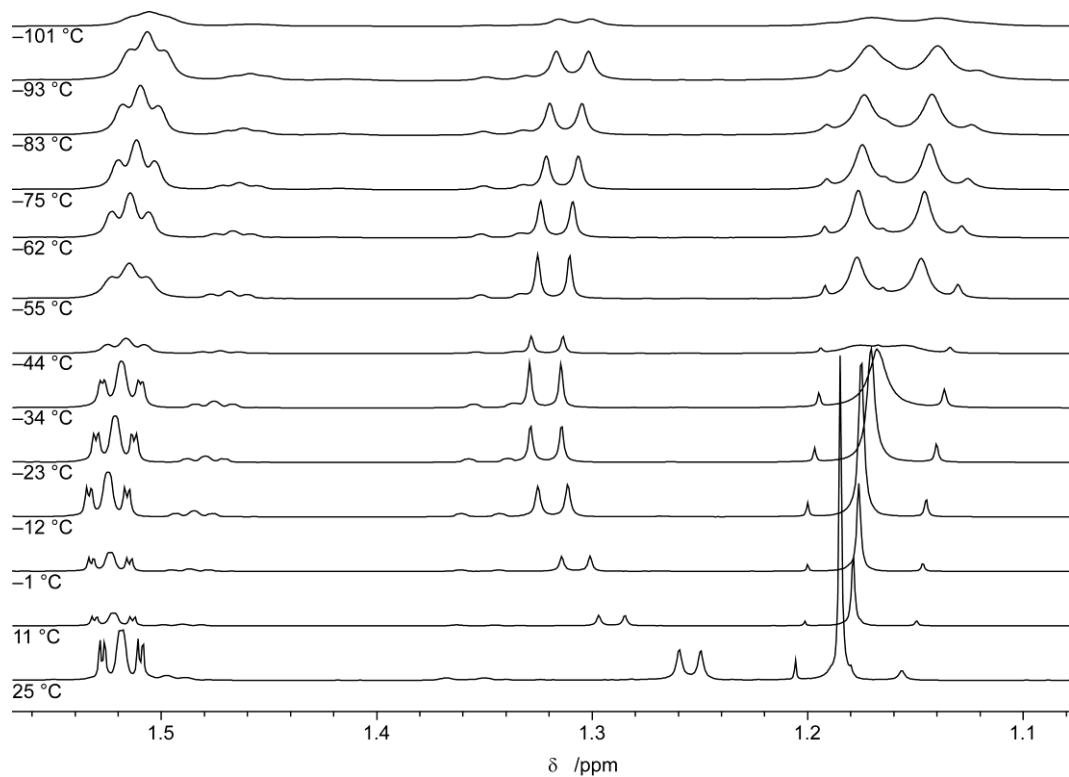


Figure S1c.3: VT-¹H NMR spectra of **2b** (400.4 MHz, THF-d₈).

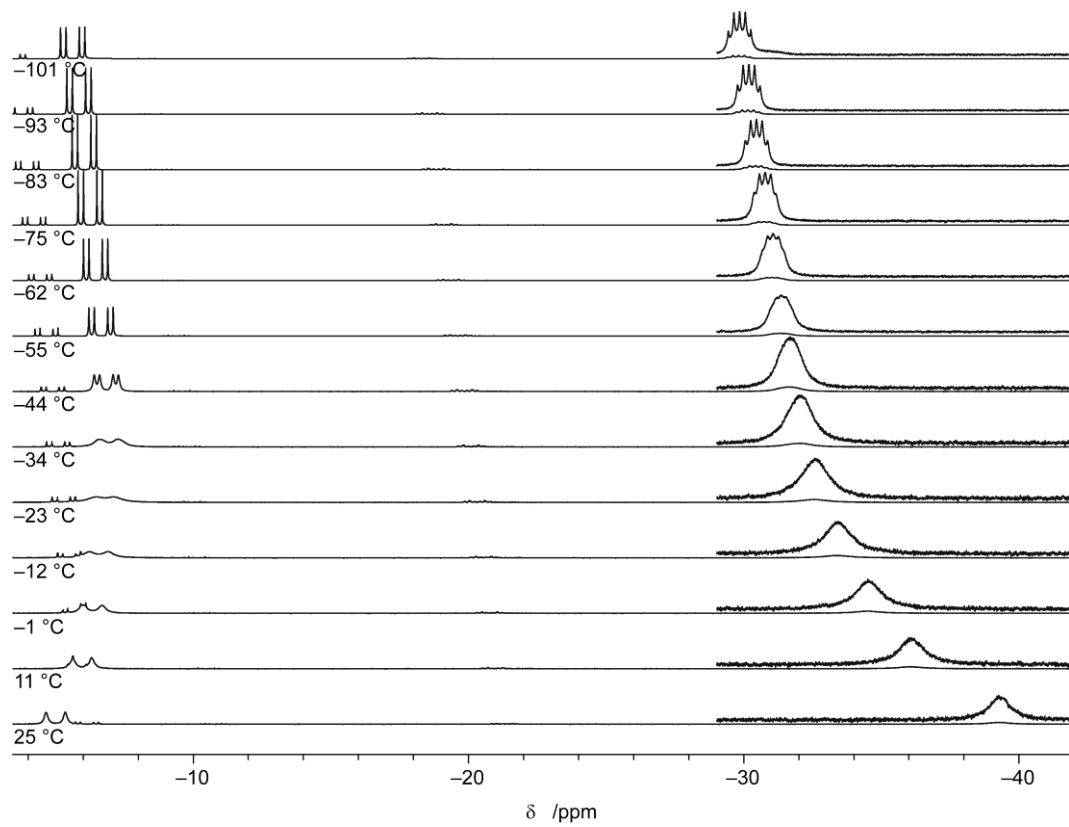


Figure S1c.4: VT-³¹P{¹H} NMR spectra of **2b** (inset: $\times 14$) (162.1 MHz, THF-d₈).

[Rh(PMe₃)₃(Bpin)₂Cl] (3b)

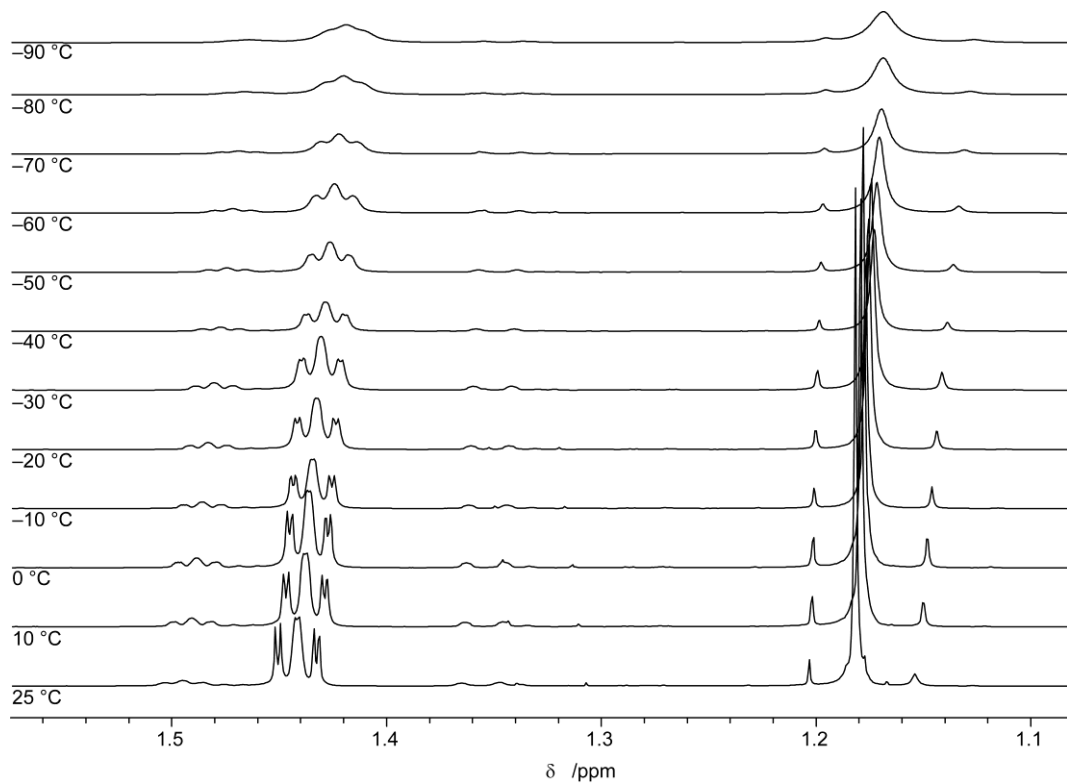


Figure S1c.5: VT-¹H NMR spectra of **3b** (400.4 MHz, THF-d₈).

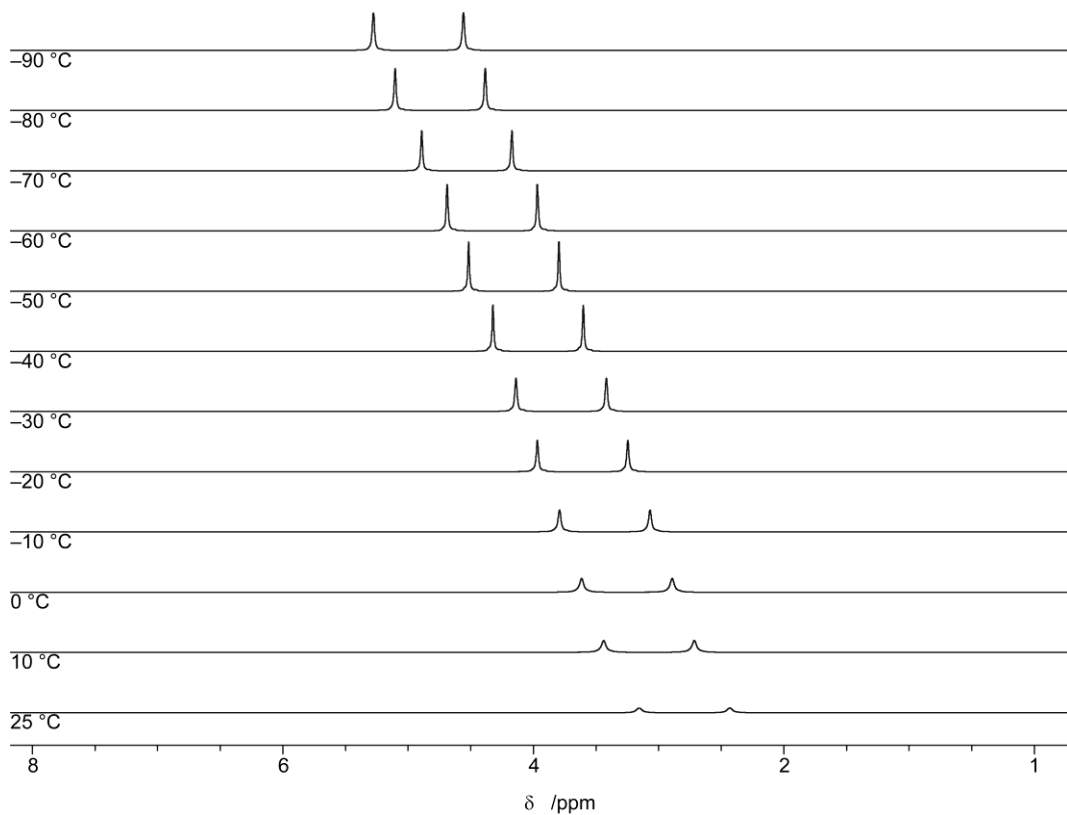


Figure S1c.6: VT-³¹P{¹H} NMR spectra of **3b** (162.1 MHz, THF-d₈).

[Rh(PMe₃)₃(Bpin)₂Cl]·[Rh(PMe₃)₂(Bpin)₂Cl] (2b·3b)

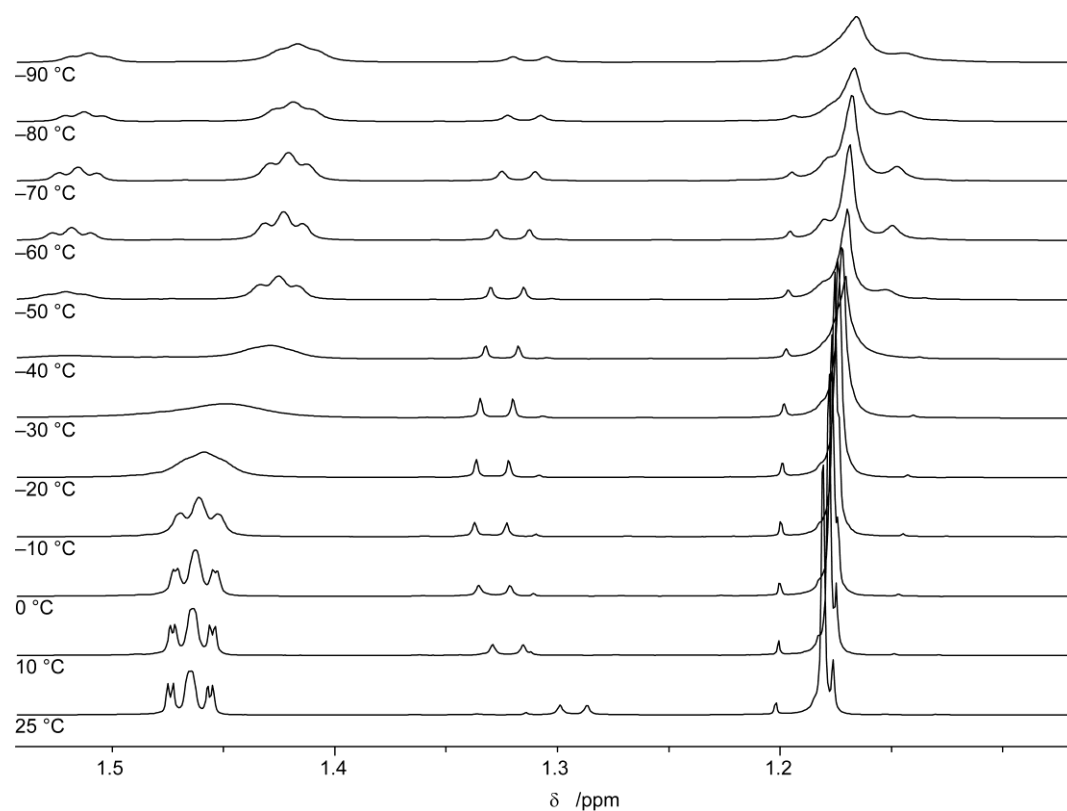


Figure S1c.7: VT-¹H NMR spectra of **2b·3b** (400.4 MHz, THF-d₈).

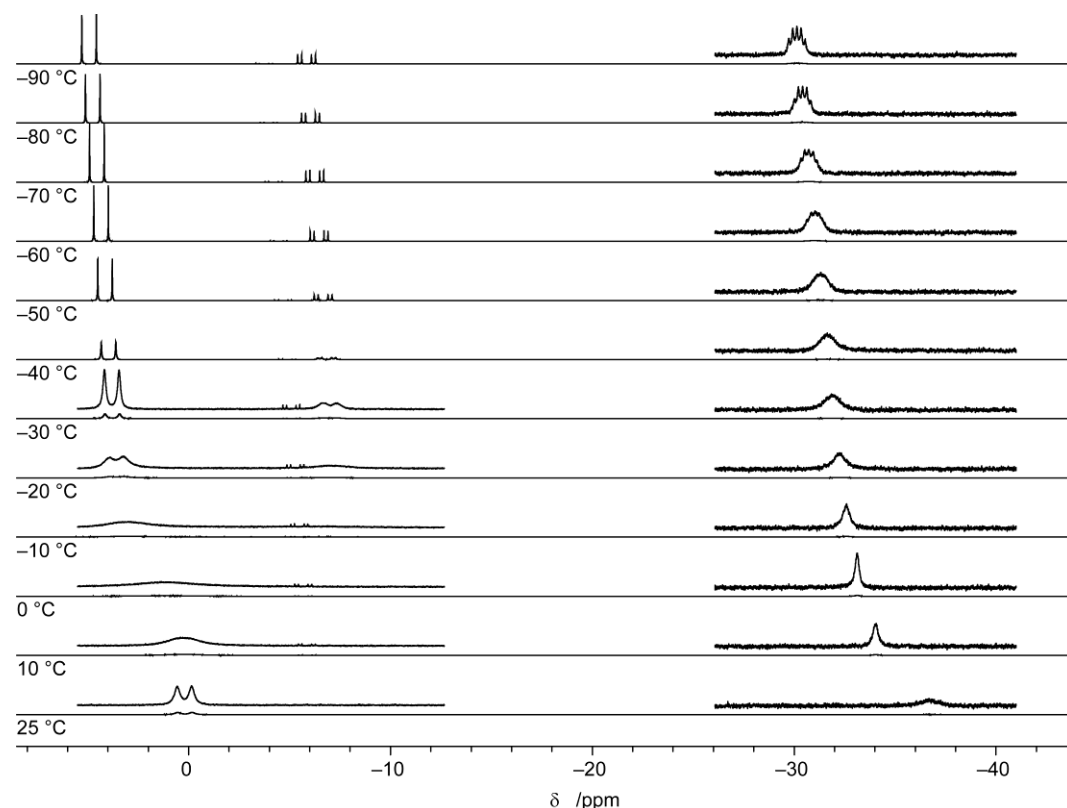


Figure S1c.8: VT-³¹P{¹H} NMR spectra of **2b·3b** (left inset: ×10, right inset: ×32) (162.1 MHz, THF-d₈).

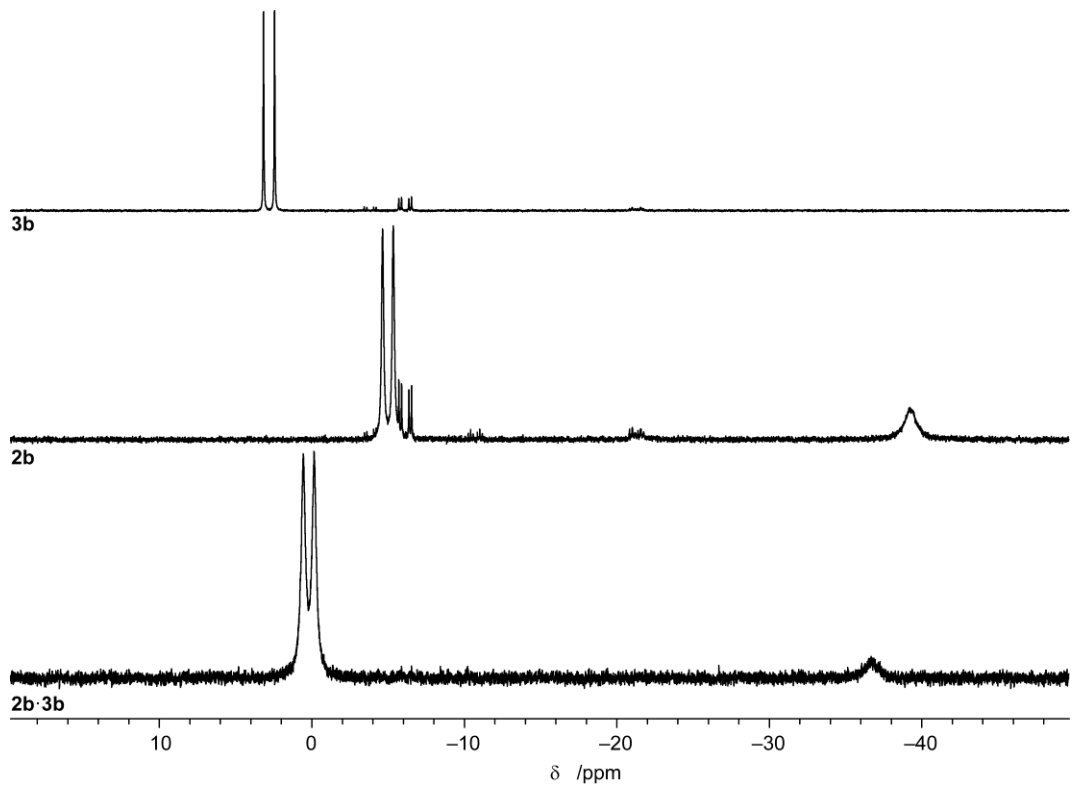


Figure S1c.9: $^{31}\text{P}\{\text{H}\}$ NMR NMR spectra of **2b-3b**, **2b** and **3b** at rt (162.1 MHz, THF- d_8).

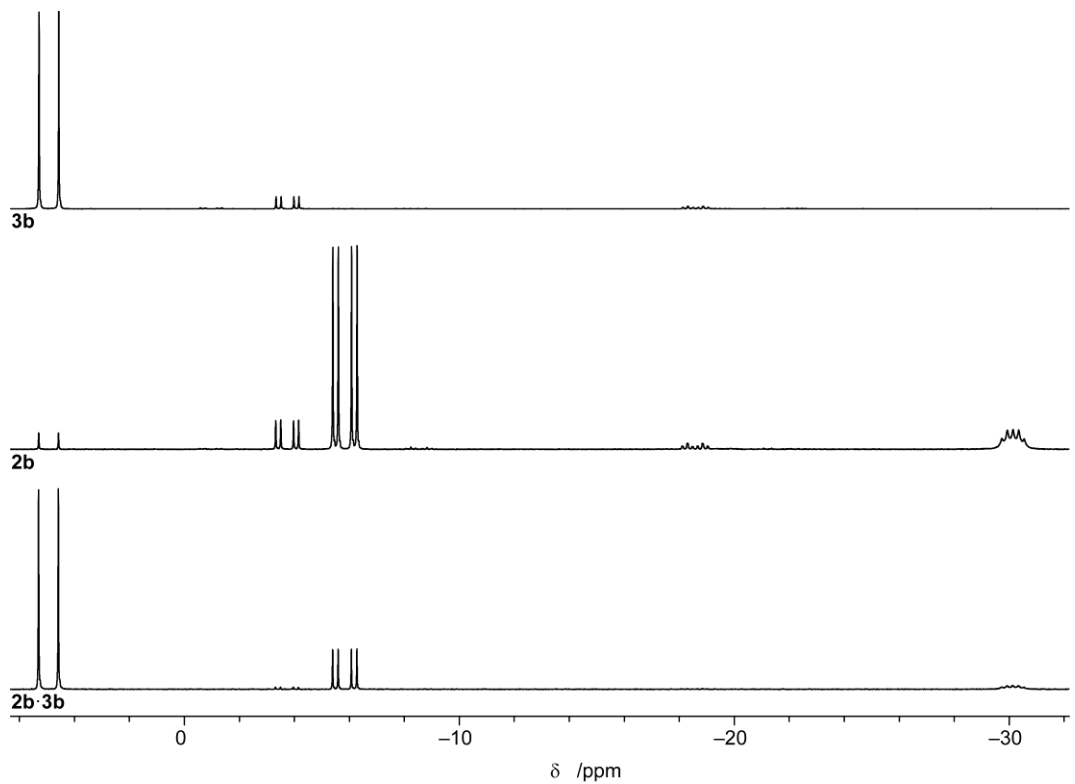


Figure S1c.10: $^{31}\text{P}\{\text{H}\}$ NMR NMR spectra of **2b-3b**, **2b** and **3b** at -90 °C (162.1 MHz, THF- d_8).

[Rh(PMe₃)₃(Bcat)(Bpin)Cl] (2c)

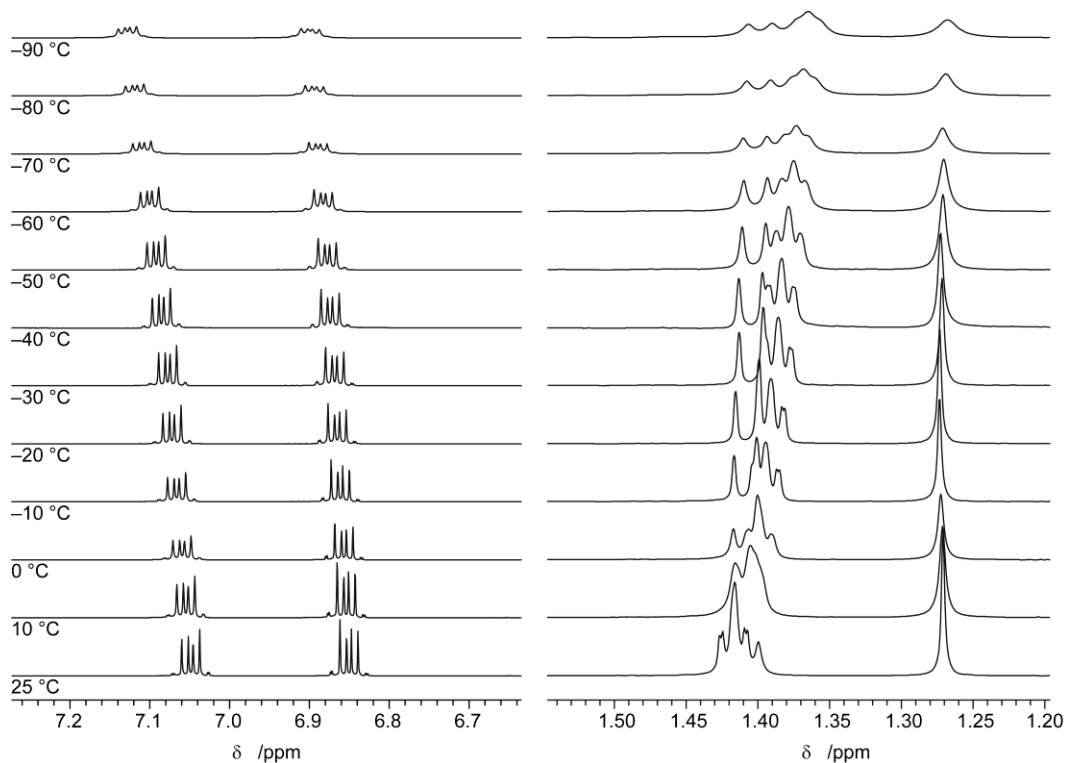


Figure S1c.11: VT-¹H NMR spectra of **2c** (400.4 MHz, THF-d₈).

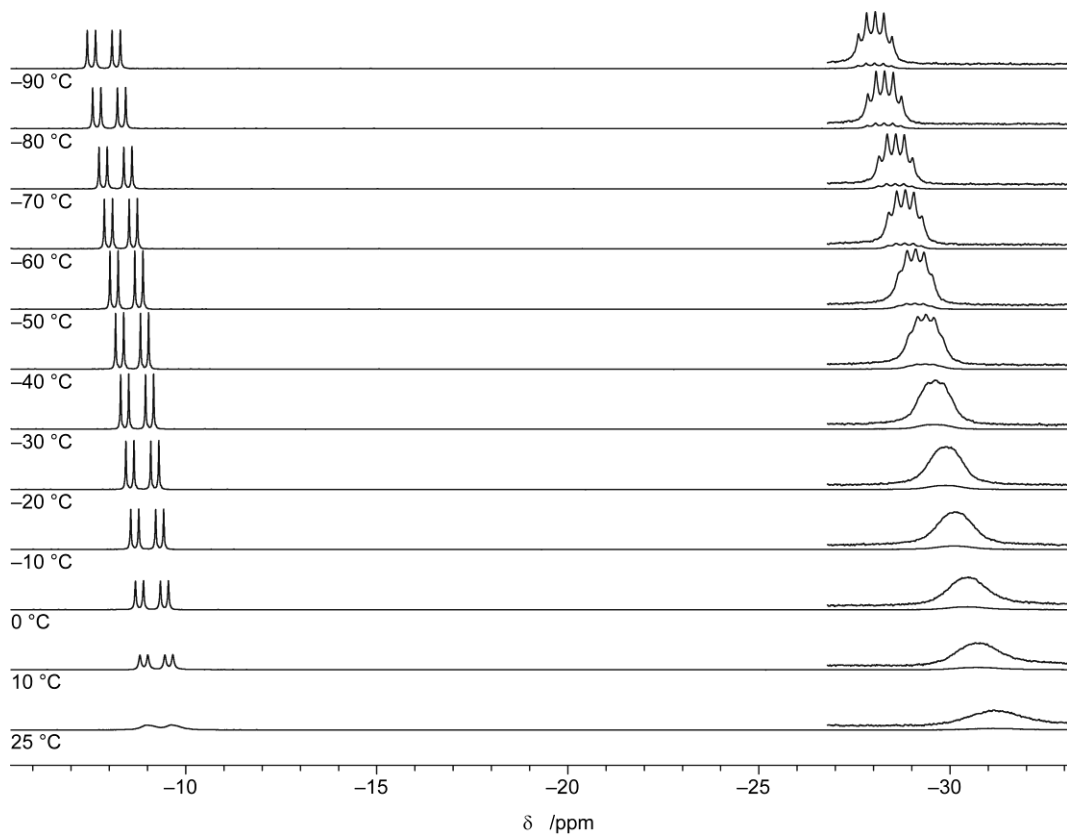


Figure S1c.12: VT-³¹P{¹H} NMR spectra of **2c** (inset: $\times 10$) (162.1 MHz, THF-d₈).

1.d. VT-NMR spectra of 4a–c, 5c, 6c

[Rh(PMe₃)₄(Bcat)₂][BArF] (4a)

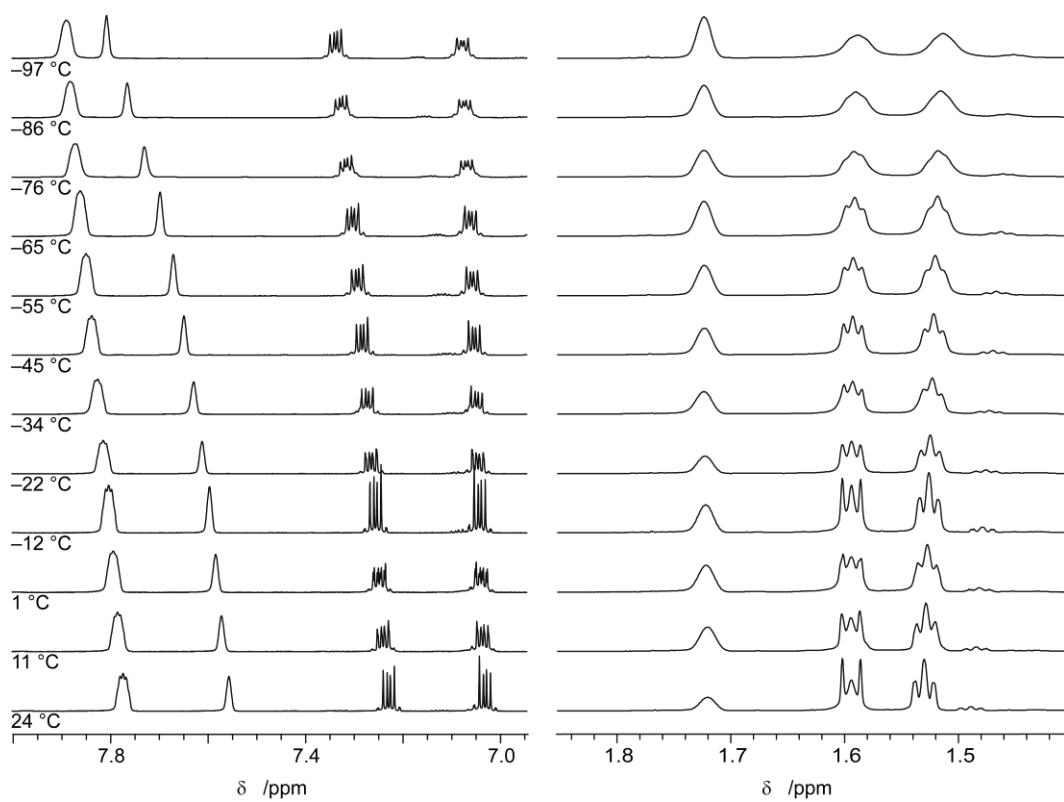


Figure S1d.1: VT-¹H NMR spectra of **4a** (400.4 MHz, THF-d₈).

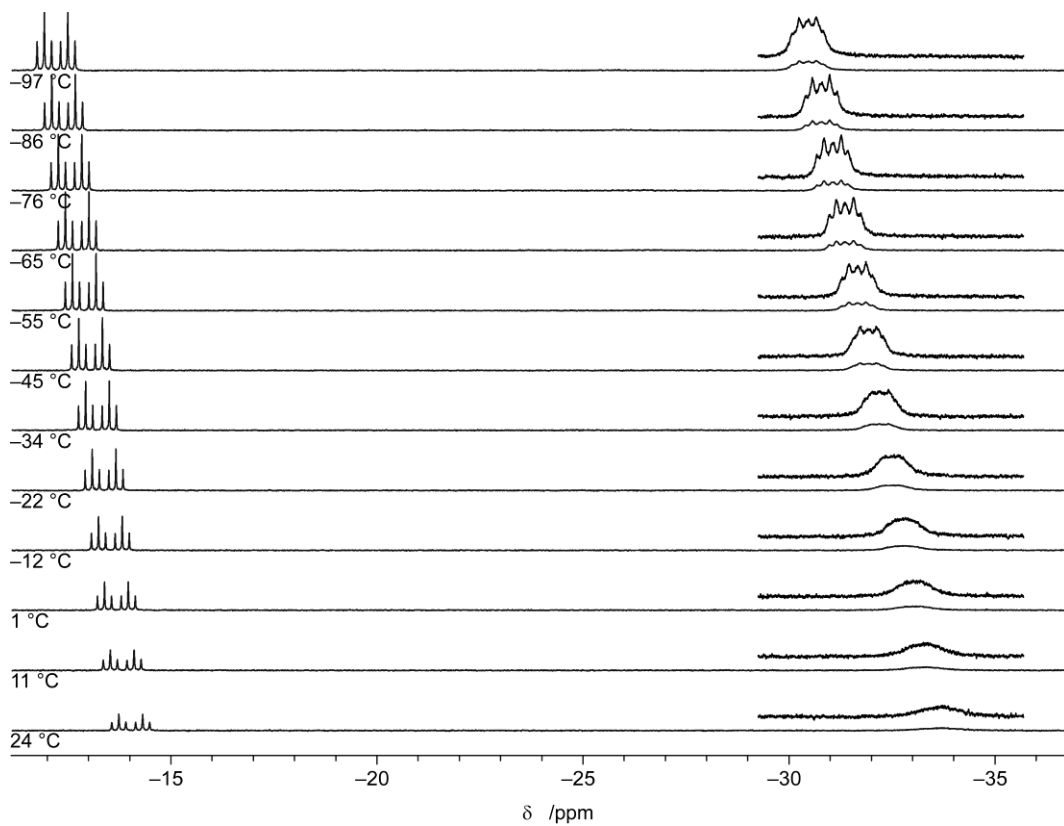


Figure S1d.2: VT-³¹P{¹H} NMR spectra of **4a** (inset: ×5) (162.1 MHz, THF-d₈).

[Rh(PMe₃)₄(Bpin)₂][BArF] (4b)

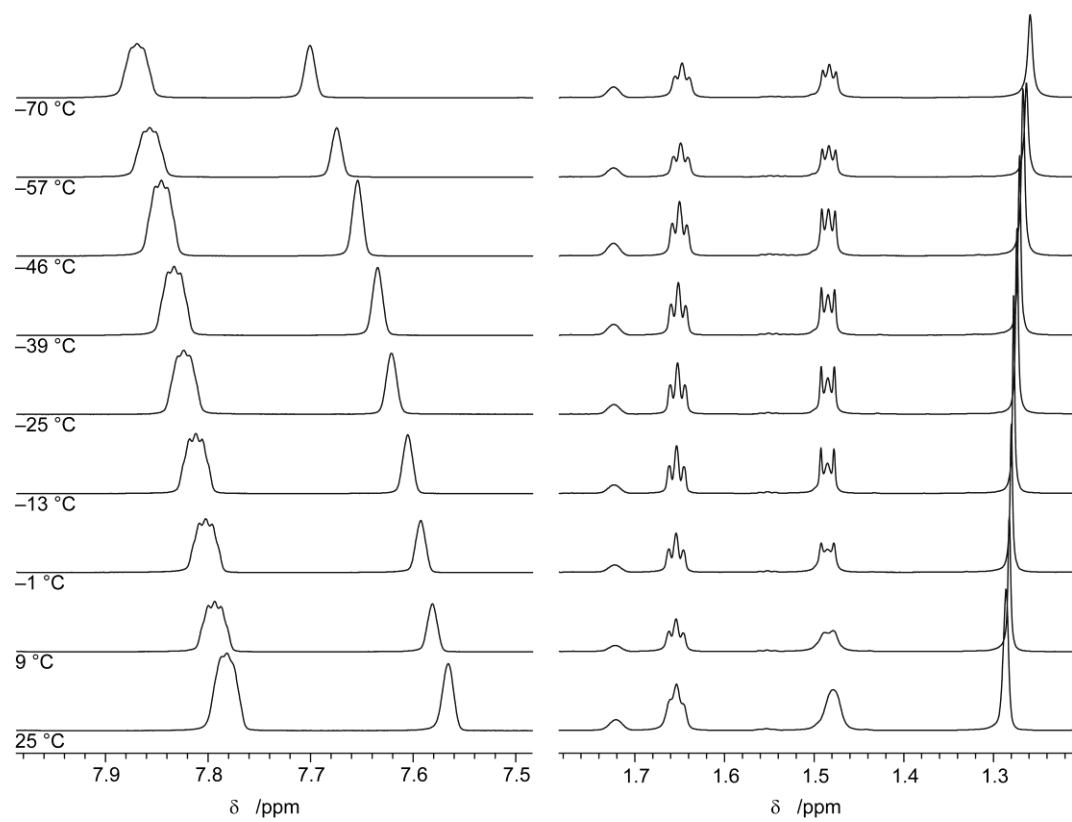


Figure S1d.3: VT-¹H NMR spectra of **4b** (400.4 MHz, THF-d₈).

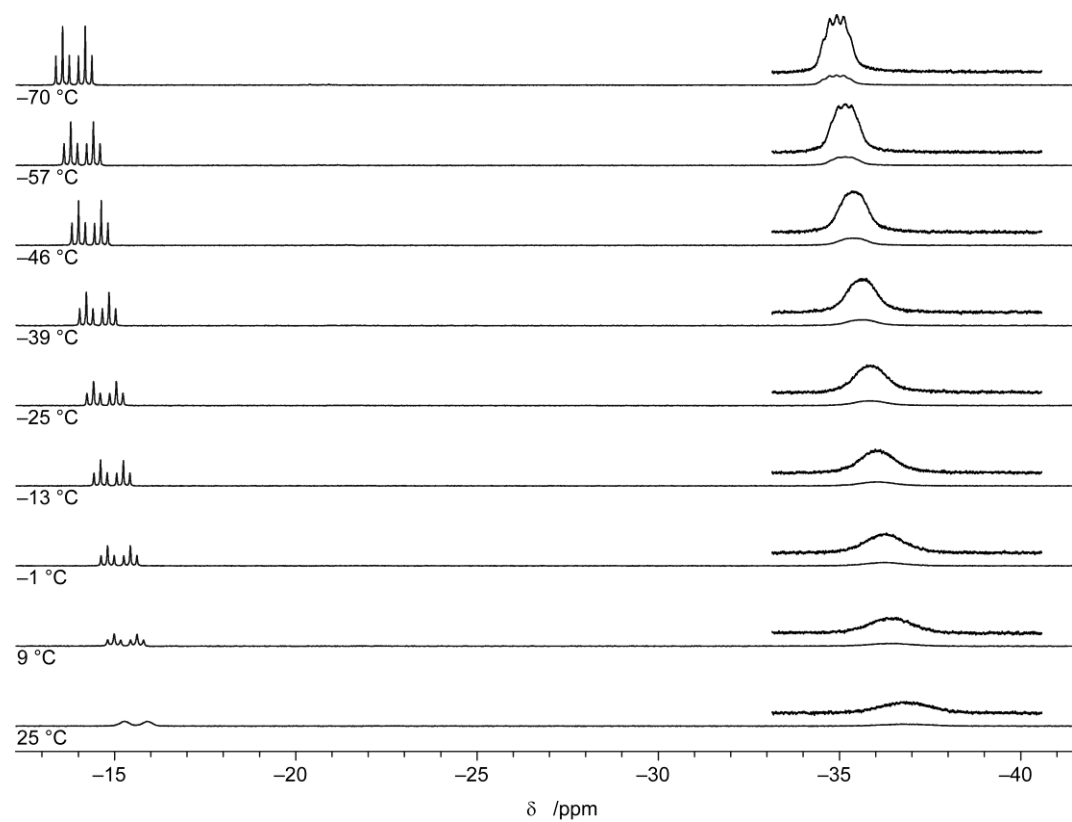


Figure S1d.4: VT-³¹P{¹H} NMR spectra of **4b** (inset: $\times 5$) (162.1 MHz, THF-d₈).

[Rh(PMe₃)₄(Bcat)(Bpin)][BArF] (4c)

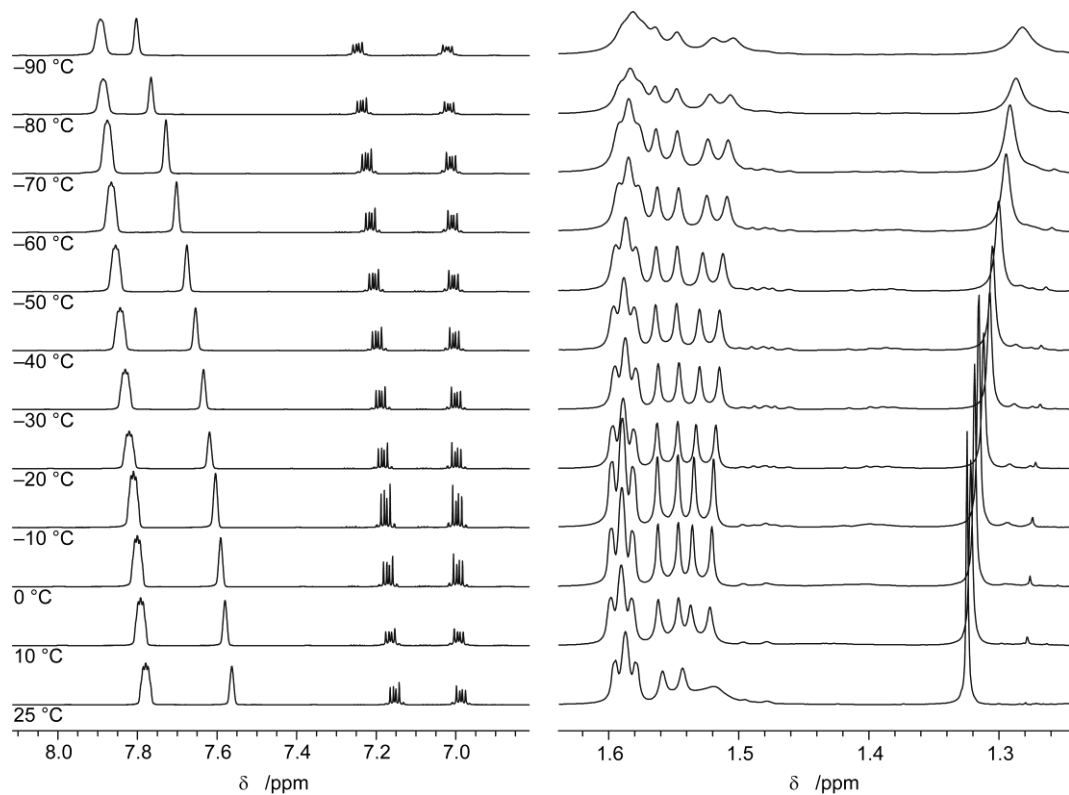


Figure S1d.5: VT-¹H NMR spectra of **4c** (400.4 MHz, THF-d₈).

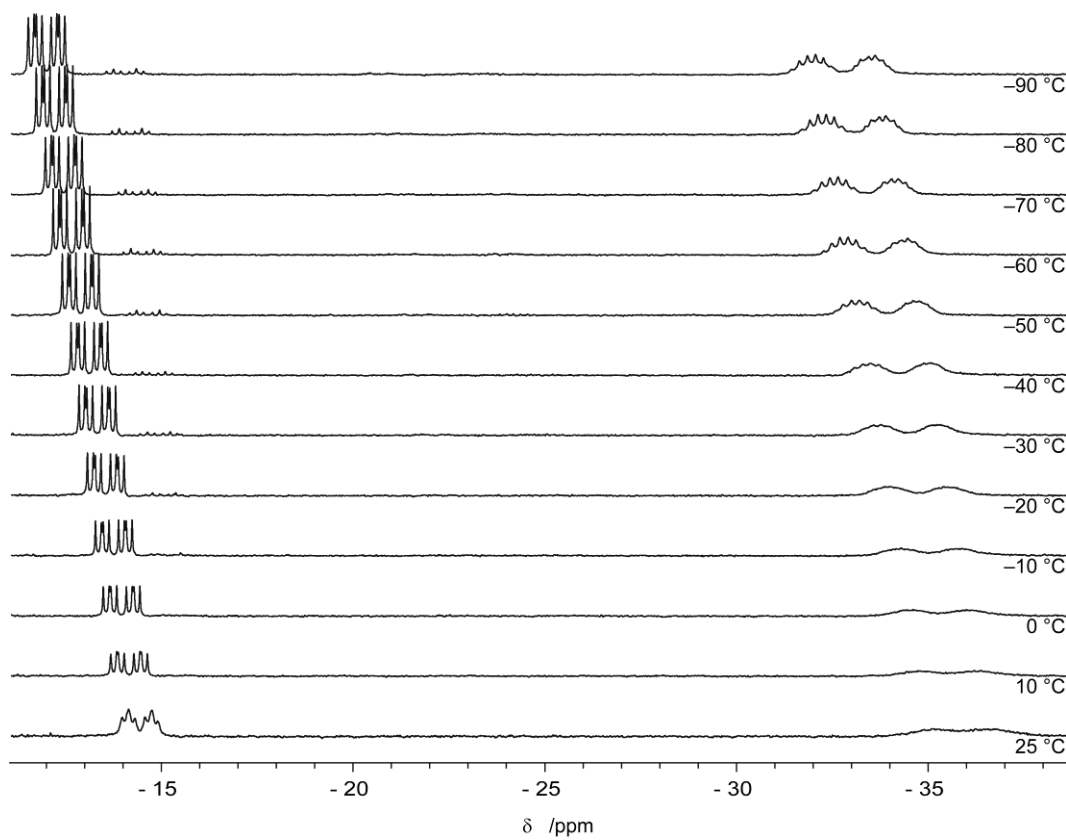


Figure S1d.6: VT-³¹P{¹H} NMR spectra of **4c** (162.1 MHz, THF-d₈).

[Rh(PMe₃)₃(NCMe)(Bcat)(Bpin)][BArF] (5c)

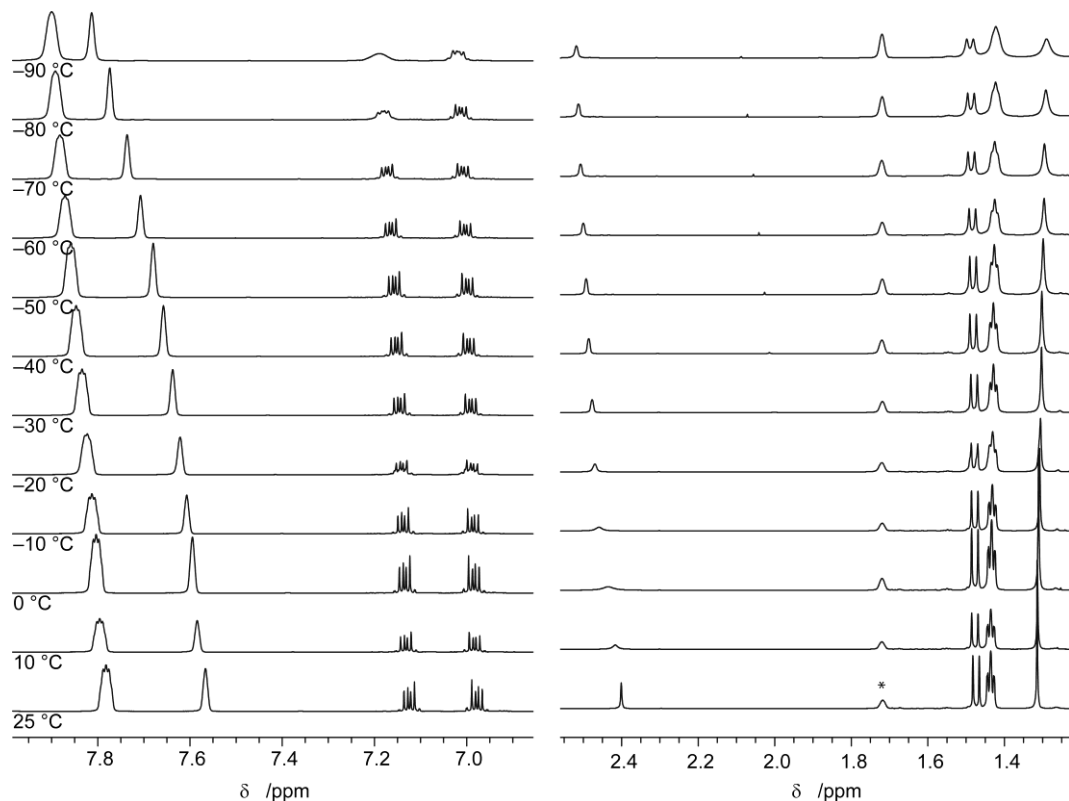


Figure S1d.7: VT-¹H NMR spectra of [Rh(PMe₃)₃(NCMe)(Bcat)(Bpin)][BArF] (5c) (400.4 MHz, THF-d₈, * denotes the residual solvent signal).

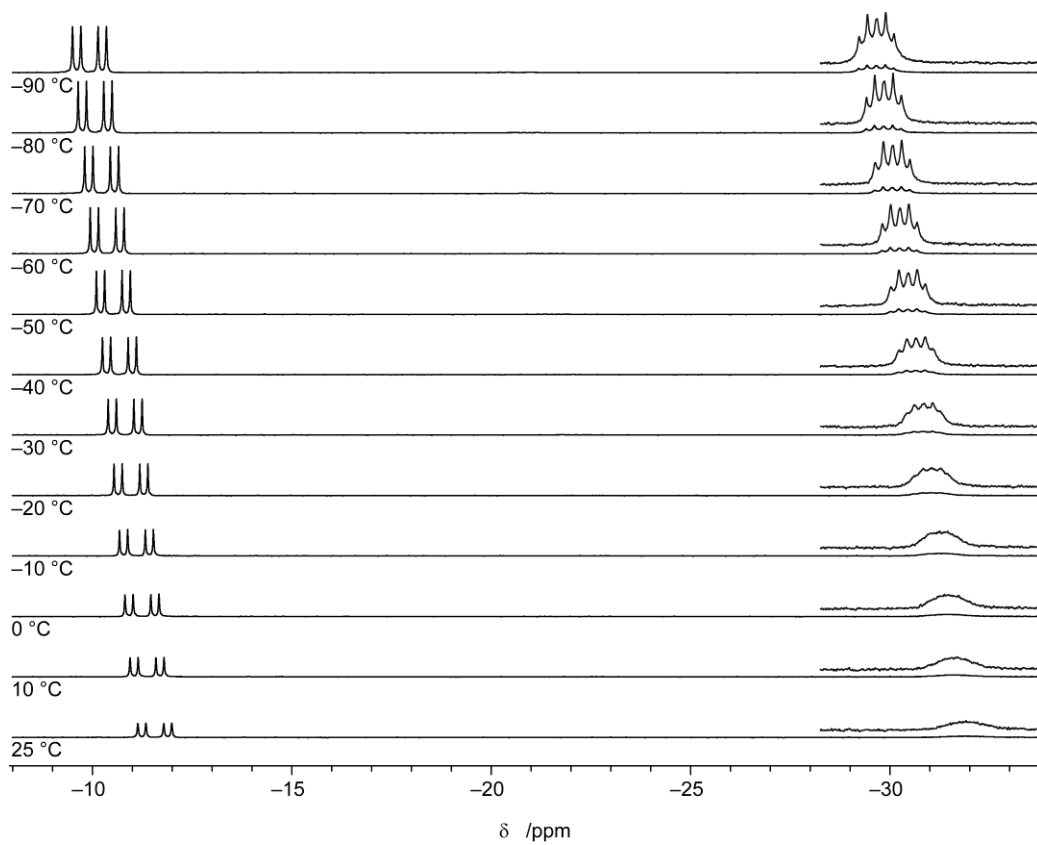


Figure S1d.8: VT-³¹P{¹H} NMR spectra of [Rh(PMe₃)₃(NCMe)(Bcat)(Bpin)][BArF] (5c) (162.1 MHz, THF-d₈).

[Rh(PMe₃)₃(CNMe)(Bcat)(Bpin)][BArF] (6c)

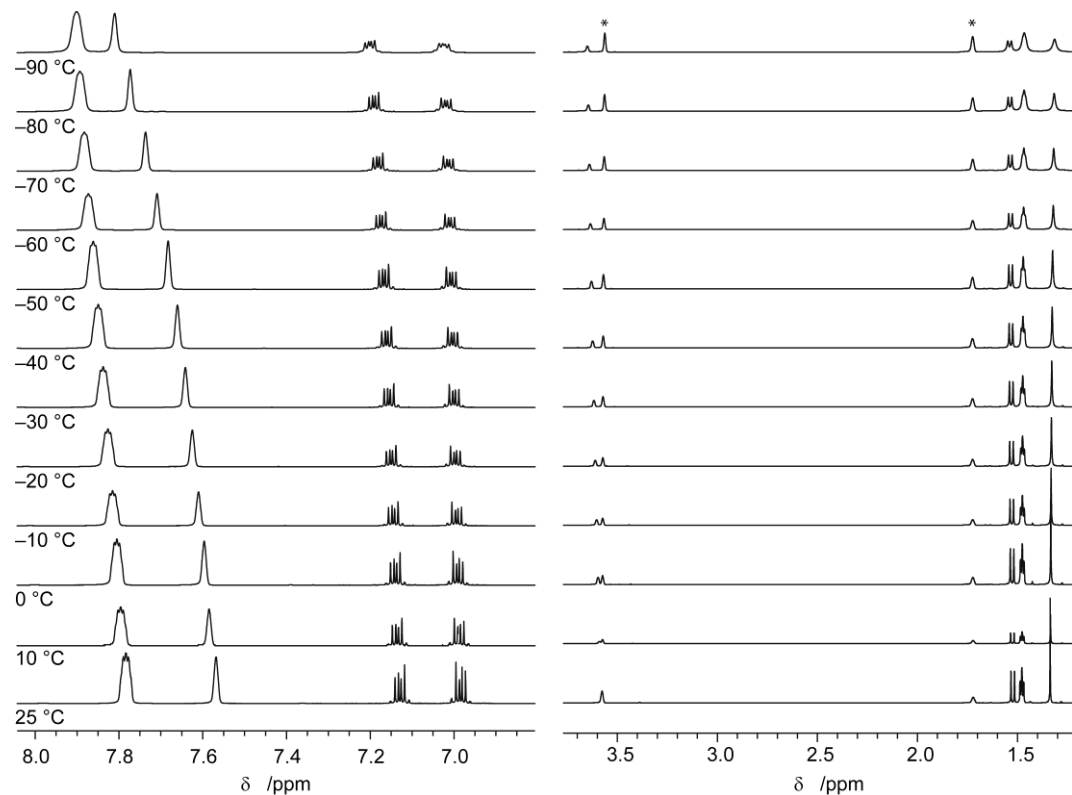


Figure S1d.9: VT-¹H NMR spectra of [Rh(PMe₃)₃(CNMe)(Bcat)(Bpin)][BArF] (**6c**) (400.4 MHz, THF-d₈, * denotes the residual solvent signal).

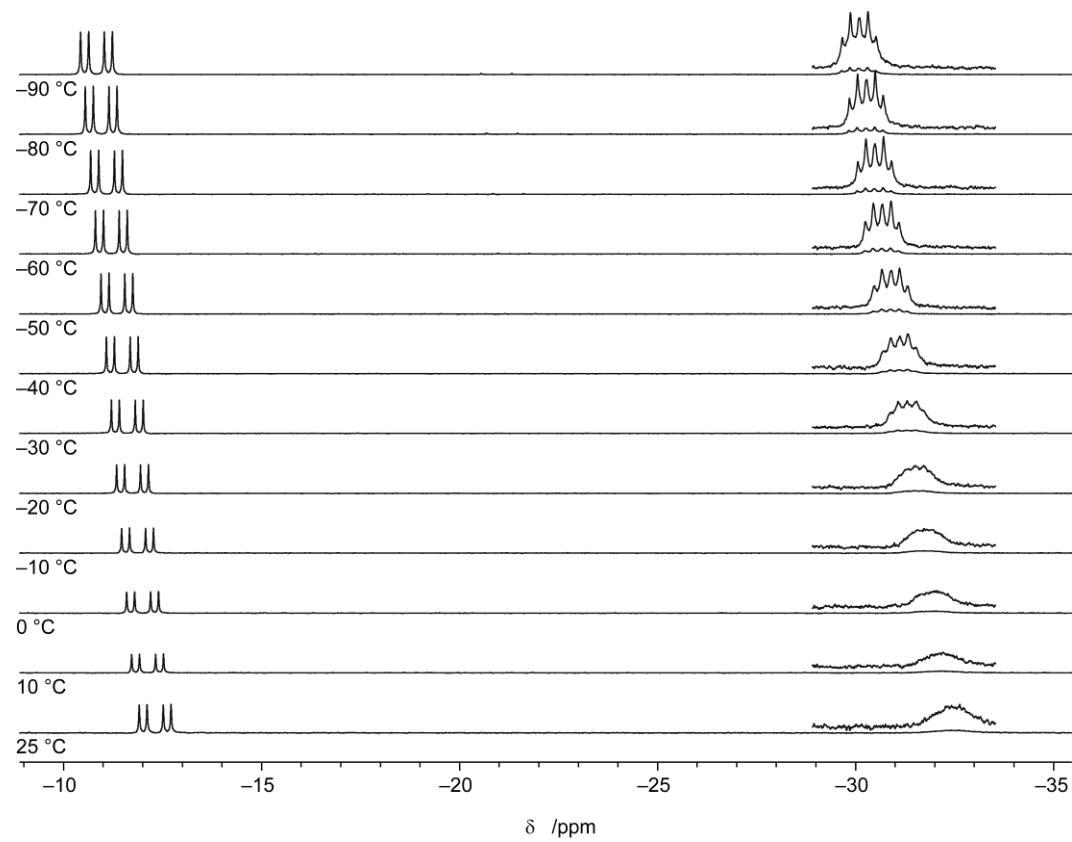


Figure S1d.10: VT-³¹P{¹H} NMR spectra of [Rh(PMe₃)₃(CNMe)(Bcat)(Bpin)][BArF] (**6c**) (162.1 MHz, THF-d₈).

2. Crystallographic Data

2.a. Crystallographic Data Collection Parameters

Table S1 Crystallographic data collection parameters for $[(\text{Me}_3\text{P})_4\text{RhH}(\text{Cl})][\text{B}(1,2-\text{O}_2\text{C}_6\text{Br}_4)_2](\text{THF})$, **2a** and **2b(PhMe)**.

	$[(\text{Me}_3\text{P})_4\text{RhH}(\text{Cl})]$ $[\text{B}(1,2-\text{O}_2\text{C}_6\text{H}_4)_2](\text{THF})^a$	2a	2b(PhMe)
Chemical Formula	$[\text{C}_{12}\text{H}_{36}\text{ClP}_4\text{Rh}][\text{C}_{12}\text{H}_8\text{BO}_4]$, $\text{C}_4\text{H}_8\text{O}$	$\text{C}_{21}\text{H}_{35}\text{B}_2\text{ClO}_4\text{P}_3\text{Rh}$	$\text{C}_{21}\text{H}_{51}\text{B}_2\text{ClO}_4\text{P}_3\text{Rh}$, C_7H_8
Formula mass (g mol ⁻¹)	741.74	604.38	712.64
Crystal shape	fragment	plate	cuboid
Crystal color	clear pale yellow	clear colourless	clear colourless
Crystal size (mm ³)	$0.088 \times 0.061 \times 0.038$	$0.246 \times 0.141 \times 0.017$	$0.205 \times 0.173 \times 0.078$
Temp., Radiation	100 K, CuK α	100 K, MoK α	100 K, MoK α
Abs. coefficient (corr.)	6.638 mm ⁻¹ (gaussian)	0.936 mm ⁻¹ (multi-scan)	0.718 mm ⁻¹ (multi-scan)
Crystal system	orthorhombic	monoclinic	monoclinic
Space group type (no.)	$P\text{ca}2_1$ (29)	$P2_1/n$ (14)	$C2/c$ (15)
Z, Z'	8, 2	4, 1	8, 1
a (Å)	33.9797(7)	8.9802(1)	32.6373(2)
b (Å)	15.7885(4)	32.0928(6)	9.7784(1)
c (Å)	13.0676(3)	9.3574(2)	22.3405(2)
α (°)	90°	90°	90°
β (°)	90°	92.003(2)°	90.123(1)°
γ (°)	90°	90°	90°
Volume (Å ³)	7010.6(3)	2695.15(8)	7129.7(1)
Refl. collected	166289	217706	1237740
unique	14341	11930	19482
observed [$I > 2\sigma(I)$]	12946	10966	17697
Data collection ranges	$3.09^\circ < \theta < 78.52^\circ$ $-43 \leq h \leq 43$ $-19 \leq k \leq 17$ $-16 \leq l \leq 16$	$2.60^\circ < \theta < 35.08^\circ$ $-14 \leq h \leq 14$ $-51 \leq k \leq 51$ $-15 \leq l \leq 15$	$2.80^\circ < \theta < 38.36^\circ$ $-56 \leq h \leq 56$ $-16 \leq k \leq 16$ $-38 \leq l \leq 39$
Completeness (to θ)	97.7% (67.7°)	100.0% (35.1°)	99.8% (38.4°)
Data / restr. / param.	14341 / 1 / 746	11930 / 0 / 298	19482 / 0 / 370
R_{int}	0.1110	0.0556	0.0702
R_1 [$I > 2\sigma(I)$]	0.0680	0.0289	0.0186
wR_2 (all data)	0.1987	0.0745	0.0456
GoF on F ²	1.055	1.172	1.042
Largest peak/hole (Å ⁻³)	2.028 / -1.202	1.441 / -1.771	0.609 / -0.473
Abs. struct. par. (Friedel cov.)	0.482(2) (86.8%)	n/a	n/a
CCDC no.	2129858	2129861	2129871

- a Due to crystal decomposition during the measurement a completeness of only 97% was obtained. The crystal was refined as a two-component inversion twin. Large unaccounted residual electron density is located at both rhodium atoms, possibly an effect of imperfect absorption correction using soft Cu radiation. However, no significant residual electron density was found in a position an expected hydrido ligand would occupy, but the presence of this additional hydrido ligand is proposed on the basis of analogy to the reported structure of $[(\text{Me}_3\text{P})_4\text{RhH}(\text{Cl})][\text{B}(1,2-\text{O}_2\text{C}_6\text{Br}_4)_2]$.^{S1}

Table S1 cont'd. Crystallographic data collection parameters for **2c**(THF)_½, **2b**·**3b** and **4a**(PhMe).

	2c (THF) _½ ^a	2b · 3b	4a (PhMe)
Chemical Formula	C ₂₁ H ₄₃ B ₂ ClO ₄ P ₃ Rh, (C ₄ H ₈ O) _½	C _{19.5} H _{46.5} B ₂ ClO ₄ P _{2.5} Rh	[C ₂₄ H ₄₄ B ₂ O ₄ P ₄ Rh] [C ₃₂ H ₁₂ BF ₂₄](C ₇ H ₈)
Formula mass (g mol ⁻¹)	648.49	582.47	1600.36
Crystal shape	cuboid	block	rhombohedron
Crystal color	clear colourless	clear colourless	clear colourless
Crystal size (mm ³)	0.243 × 0.177 × 0.067	0.391 × 0.276 × 0.174	0.252 × 0.116 × 0.035
Temp., Radiation	100 K, MoK α	100 K, MoK α	100 K, MoK α
Abs. coefficient (corr.)	0.814 mm ⁻¹ (numerical)	0.857 mm ⁻¹ (multi-scan)	0.449 mm ⁻¹ (gaussian)
Crystal system	orthorhombic	triclinic	triclinic
Space group type (no.)	<i>Pbcn</i> (60)	<i>P</i> 1 (2)	<i>P</i> 1 (2)
Z, Z'	8, 1	8, 4	2, 1
<i>a</i> (Å)	34.795(1)	17.6266(2)	13.0318(3)
<i>b</i> (Å)	13.2910(4)	19.1196(2)	13.3464(3)
<i>c</i> (Å)	13.5036(4)	19.3690(2)	20.4288(5)
α (°)	90°	60.968(1)°	79.347(2)°
β (°)	90°	85.334(1)°	86.005(2)°
γ (°)	90°	85.987(1)°	83.375(2)°
Volume (Å ³)	6245.0(3)	5685.0(1)	3464.3(1)
Refl. collected			
unique	183646	559571	270981
observed [<i>I</i> >2σ(<i>I</i>)]	8329	59685	17205
Data collection ranges	2.23° < θ < 29.36° -46 ≤ <i>h</i> ≤ 47 -18 ≤ <i>k</i> ≤ 18 -18 ≤ <i>l</i> ≤ 18	2.63° < θ < 38.29° -30 ≤ <i>h</i> ≤ 29 -33 ≤ <i>k</i> ≤ 32 -33 ≤ <i>l</i> ≤ 33	2.62° < θ < 28.28° -17 ≤ <i>h</i> ≤ 17 -17 ≤ <i>k</i> ≤ 17 -27 ≤ <i>l</i> ≤ 27
Completeness (to θ)	99.9% (29.4°)	99.8% (25.2°)	99.9% (28.3°)
Data / restr. / param.	8329 / 96 / 339	59685 / 0 / 1143	17205 / 0 / 905
<i>R</i> _{int}	0.1009	0.0477	0.0573
<i>R</i> ₁ [<i>I</i> >2σ(<i>I</i>)]	0.0383	0.0254	0.0526
<i>wR</i> ₂ (all data)	0.0913	0.0593	0.1392
GoF on F ²	1.037	1.057	1.051
Largest peak/hole (Å ⁻³)	0.958 / -0.944	0.964 / -0.680	2.016 / -1.119
Abs. struct. par. (Friedel cov.)	n/a	n/a	n/a
CCDC no.	2129860	2129866	2129863

a DSR was used to model a disordered THF molecule.^{S2} Additionally restraints (SADI, SIMU, RIGU, ISOR) were employed.

Table S1 cont'd. Crystallographic data collection parameters for **4b**, **4c**(THF) and **3b**.

	4b	4c (THF)	3b
Chemical Formula	[C ₂₄ H ₆₀ B ₂ O ₄ P ₄ Rh] [C ₃₂ H ₁₂ BF ₂₄]	[C ₂₄ H ₅₂ B ₂ O ₄ P ₄ Rh] [C ₃₂ H ₁₂ BF ₂₄](C ₄ H ₈ O)	C ₁₈ H ₄₂ B ₂ ClO ₄ P ₂ Rh
Formula mass (g mol ⁻¹)	1524.35	1588.39	544.43
Crystal shape	fragment of plate	octahedral	needle
Crystal color	clear colourless	clear colourless	clear colourless
Crystal size (mm ³)	0.260 × 0.163 × 0.040	0.190 × 0.113 × 0.105	0.441 × 0.023 × 0.019
Temp., Radiation	100 K, MoK α	100 K, MoK α	100 K, CuK α
Abs. coefficient (corr.)	0.463 mm ⁻¹ (multi-scan)	0.446 mm ⁻¹ (gaussian)	7.222 mm ⁻¹ (gaussian)
Crystal system	monoclinic	monoclinic	trigonal
Space group type (no.)	P ₂ 1/n (14)	P ₂ 1/n (14)	R3c (161)
Z, Z'	4, 1	4, 1	18, 1
a (Å)	21.7869(7)	14.8031(4)	34.921(2)
b (Å)	13.4146(3)	26.6122(8)	34.921(2)
c (Å)	24.8701(8)	17.8342(4)	11.6219(8)
α (°)	90°	90°	90°
β (°)	113.690(4)°	95.991(2)°	90°
γ (°)	90°	90°	120°
Volume (Å ³)	6656.1(4)	6987.3(3)	12274.1(15)
Refl. collected	260578	84638	23803
unique	20196	18834	4133
observed [$I > 2\sigma(I)$]	16699	15872	3799
Data collection ranges	2.54° < θ < 30.49° −31 ≤ h ≤ 30 −19 ≤ k ≤ 17 −35 ≤ l ≤ 35	1.89° < θ < 31.28° −19 ≤ h ≤ 19 −36 ≤ k ≤ 36 −25 ≤ l ≤ 25	2.53° < θ < 66.60° −41 ≤ h ≤ 41 −40 ≤ k ≤ 41 −13 ≤ l ≤ 10
Completeness (to θ)	99.5% (30.5°)	99.7% (27.0°)	100.0% (66.6°)
Data / restr. / param.	20196 / 0 / 877	18834 / 0 / 900	4133 / 1 / 267
R_{int}	0.0893	0.0385	0.1133
R_1 [$I > 2\sigma(I)$]	0.0580	0.0383	0.0654
wR ₂ (all data)	0.1323	0.0916	0.1767
GoF on F ²	1.129	1.014	1.053
Largest peak/hole (Å ⁻³)	1.103 / −1.599	1.090 / −0.892	2.059 / −0.757
Abs. struct. par. (Friedel cov.)	n/a	n/a	−0.02(2)
CCDC no.	2129865	2129864	2129859

Table S1 cont'd. Crystallographic data collection parameters for
 $[\text{Rh}(\text{PPh}_3)_2(\text{Bcat})(\text{Bpin})(\text{Cl})] \cdot (\text{dcm})_{3.5}(\text{C}_5\text{H}_{12})_{0.5}$, **5c** and **6c(THF)_{0.53}(C₅H₁₂)_{0.47}**.

	$[\text{Rh}(\text{PPh}_3)_2(\text{Bcat})(\text{Bpin})(\text{Cl})]$ $\cdot (\text{dcm})_{3.5}(\text{C}_5\text{H}_{12})_{0.6}^{\text{a}}$	5c	6c(THF)_{0.53}(C₅H₁₂)_{0.47}
Chemical Formula	$[\text{C}_{48}\text{H}_{45}\text{B}_2\text{ClO}_4\text{P}_2\text{Rh}]$ $(\text{CH}_2\text{Cl}_2)_{3.5} \cdot (\text{C}_5\text{H}_{12})_{0.6}$	$[\text{C}_{23}\text{H}_{46}\text{B}_2\text{NO}_4\text{P}_3\text{Rh}]$ $[\text{C}_{32}\text{H}_{12}\text{BF}_{24}]$	$[\text{C}_{23}\text{H}_{46}\text{B}_2\text{NO}_4\text{P}_3\text{Rh}]$ $[\text{C}_{32}\text{H}_{12}\text{BF}_{24}]$
Formula mass (g mol ⁻¹)	1248.41	1481.27	1553.39
Crystal shape	block	cuboid	block
Crystal color	clear orange	clear colourless	clear colourless
Crystal size (mm ³)	0.697 × 0.455 × 0.411	0.214 × 0.109 × 0.088	0.210 × 0.167 × 0.090
Temp., Radiation	102 K, MoK α	100 K, MoK α	100 K, MoK α
Abs. coefficient (corr.)	0.767 mm ⁻¹ (multi-scan)	0.452 mm ⁻¹ (multi-scan)	0.444 mm ⁻¹ (multi-scan)
Crystal system	monoclinic	monoclinic	monoclinic
Space group type (no.)	<i>P</i> 2 ₁ / <i>n</i> (14)	<i>P</i> 2 ₁ / <i>c</i> (14)	<i>P</i> 2 ₁ / <i>c</i> (14)
Z, Z'	4, 1	4, 1	4, 1
a (Å)	11.2915(2)	18.0677(3)	20.9665(3)
b (Å)	21.8994(4)	13.9610(2)	13.5826(1)
c (Å)	23.4243(5)	25.9822(4)	26.9822(4)
α (°)	90°	90°	90°
β (°)	95.632(2)°	99.739(2)°	112.321(2)°
γ (°)	90°	90°	90°
Volume (Å ³)	5764.3(2)	6459.4(2)	6948.0(1)
Refl. collected	356179	281801	656079
unique	20671	24676	27493
observed [$I > 2\sigma(I)$]	17785	19168	22605
Data collection ranges	2.29° < θ < 32.98° $-16 \leq h \leq 16$ $-32 \leq k \leq 33$ $-35 \leq l \leq 35$	2.56° < θ < 34.23° $-26 \leq h \leq 28$ $-20 \leq k \leq 21$ $-40 \leq l \leq 39$	1.60° < θ < 34.23° $-33 \leq h \leq 28$ $-20 \leq k \leq 21$ $-41 \leq l \leq 40$
Completeness (to θ)	99.9% (30.0°)	99.9% (25.2°)	99.9% (25.2°)
Data / restr. / param.	20671 / 327 / 751	24676 / 0 / 834	0371 / 64 / 993
R_{int}	0.0443	0.0334	0.0556
R_1 [$I > 2\sigma(I)$]	0.0375	0.0428	0.0371
wR ₂ (all data)	0.0839	0.1128	0.0948
GoF on F ²	1.083	1.035	1.035
Largest peak/hole (Å ⁻³)	0.876 / -0.683	1.729 / -1.093	0.950 / -0.387
Abs. struct. par. (Friedel cov.)	n/a	n/a	n/a
CCDC no.	2129862	2129867	2129870

- a The crystal was handled below -40 °C throughout the mounting process using an X-temp 2 apparatus. The crystal was mounted on top of a glass fibre in perfluoroether oil and placed in a cold nitrogen gas stream on the diffractometer at -171 °C.^{S3}
Three (disordered) CH₂Cl₂ moieties were refined applying split atom models, applying geometrical restraints on C–Cl distances (DFIX); certain atom pairs were refined with a common ADP (EADP).
An initial refinement of residual electron density suggested the presence of disordered CH₂Cl₂/C₅H₁₂ in an approximate 1:1.2 ratio. No appropriate model could be established for these disordered CH₂Cl₂/n-pentane molecules; the data were processed using the BYPASS algorithm as implemented in OLEX2.^{S4,5}

2.b. $[(\text{Me}_3\text{P})_4\text{RhH}(\text{Cl})][\text{B}(1,2-\text{O}_2\text{C}_6\text{H}_4)_2](\text{THF})$

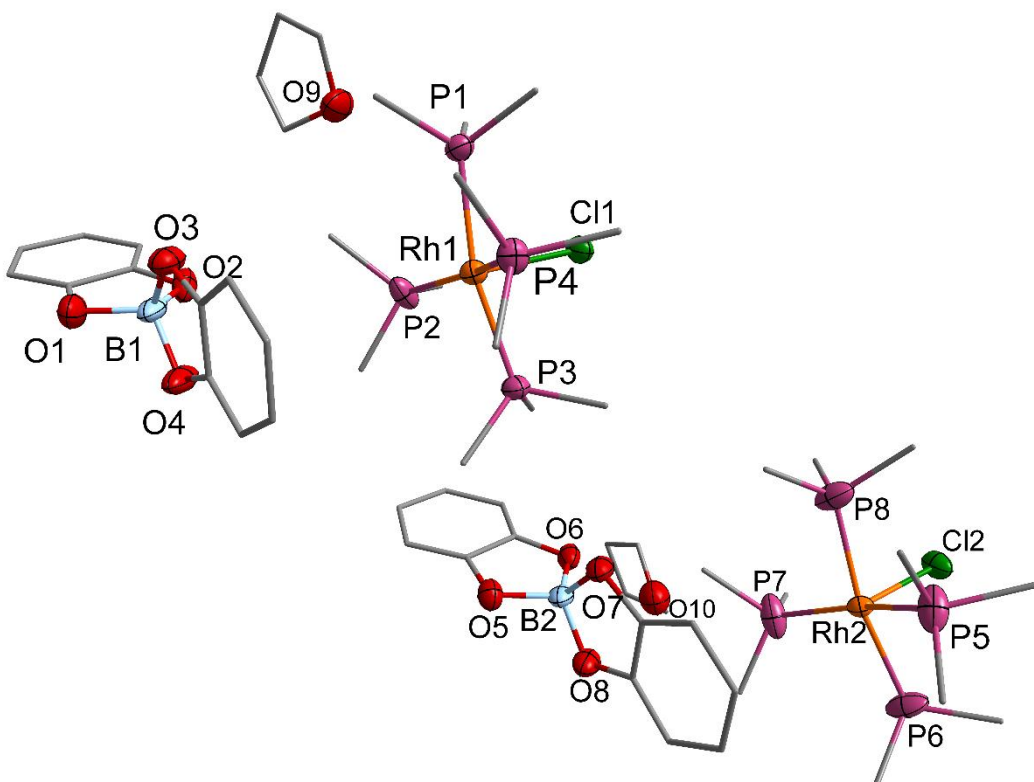


Figure S2b.1 Asymmetric unit of $[(\text{Me}_3\text{P})_4\text{RhH}(\text{Cl})][\text{B}(1,2-\text{O}_2\text{C}_6\text{H}_4)_2](\text{THF})$. Selected distances (\AA) and angles ($^\circ$): Rh1–Cl1 2.487(2), Rh1–P1 2.342(2), Rh1–P2 2.328(2), Rh1–P3 2.334(2), Rh1–P4 2.328(2), P1–Rh1–P3 165.26(9), P2–Rh1–P4 158.01(9); Rh2–Cl2 2.490(2), Rh2–P5 2.312(3), Rh2–P6 2.346(3), Rh2–P7 2.342(3), Rh2–P8 2.314(3), P5–Rh2–P7 165.8(1), P6–Rh2–P8 158.8(1).

The solid-state structure of the cation $[(\text{Me}_3\text{P})_4\text{RhH}(\text{Cl})]^+$ in $[(\text{Me}_3\text{P})_4\text{RhH}(\text{Cl})][\text{B}(1,2-\text{O}_2\text{C}_6\text{H}_4)_2]$ resemble that of the ion in $[(\text{Me}_3\text{P})_4\text{RhH}(\text{Cl})][\text{B}(1,2-\text{O}_2\text{C}_6\text{Br}_4)_2]$ (Rh1–Cl1 2.51(1) \AA , Rh1–P1 2.357(2) \AA , Rh1–P2 2.345(2) \AA , Rh1–P3 2.343(2) \AA , Rh1–P4 2.322(2) \AA , P1–Rh1–P3 166.27(9) $^\circ$, P2–Rh1–P4 159.16(9) $^\circ$).^{S1} The geometrical similarity suggests that the both structures contain the same cation $[(\text{Me}_3\text{P})_4\text{RhH}(\text{Cl})]^+$ despite that the hydrido ligand was not identified in the X-ray structure determination of $[(\text{Me}_3\text{P})_4\text{RhH}(\text{Cl})][\text{B}(1,2-\text{O}_2\text{C}_6\text{H}_4)_2](\text{THF})$.

2.c. $[(\text{Me}_3\text{P})_2\text{Rh}(\text{Bpin})_2\text{Cl}]$ (**3b**) and **2b**-**3b**

The oxidative addition of **1b** to $[\text{Rh}(\text{PMe}_3)_3\text{Cl}]$ did not only furnished **2b** but also the five coordinate rhodium(III) complex $[\text{Rh}(\text{PMe}_3)_2(\text{Bpin})_2\text{Cl}]$ (**3b**). Two different solid state structures of **3b** were obtained, one in the trigonal space group type *R*3c comprising one molecule in the asymmetric unit ($Z = 18$, $Z' = 1$) of only mediocre quality and one of better quality co-crystallised with **2b** as **2b**-**3b** (Figure S2c.1).

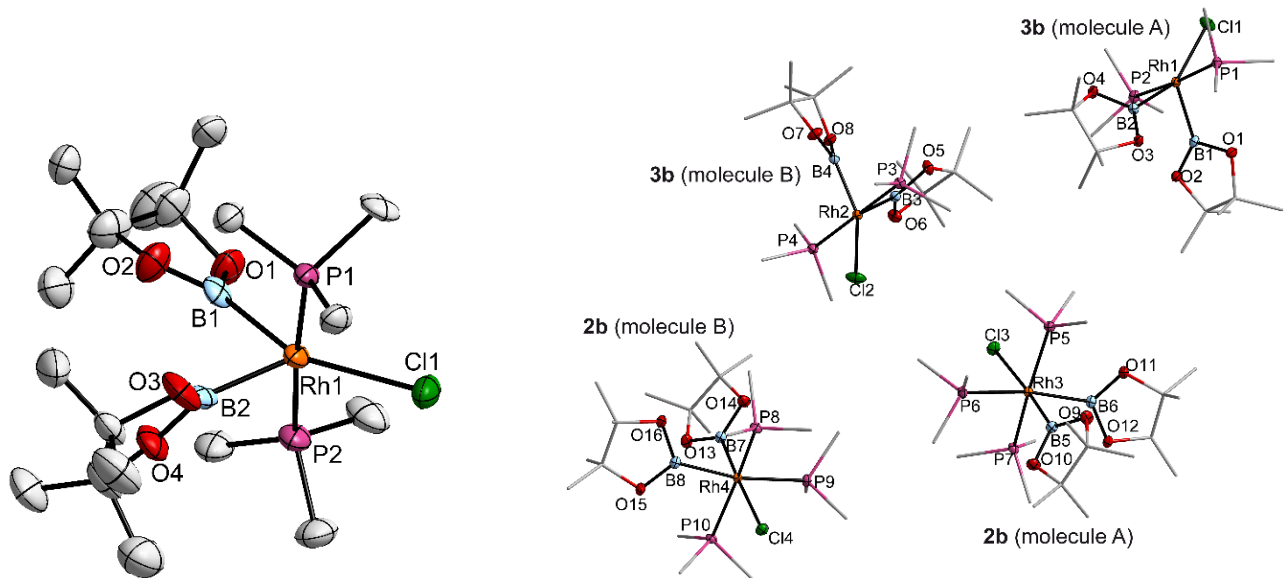


Figure S2c.1 **Left:** Molecular structures of **3b** from **3b** in *R*3c. Selected distances (\AA) and angles ($^\circ$): Rh1–Cl1 2.448(3), Rh1–P1 2.302(3), Rh1–P2 2.320(3), Rh1–B1 2.01(1), Rh1–B2 1.99(2), B1…B2 2.45(2), P1–Rh1–P2 176.1(1), B1–Rh1–Cl1 152.7(4), B2–Rh1–Cl1 131.4(4), B1–Rh1–B2 75.9(5), $\tau_{\text{B}1}$ 38(2), $\tau_{\text{B}1}$ 72(2).

Right: Asymmetric unit of the solid state structure of **2b**-**3b**. Selected geometrical data of **3b** [\AA / $^\circ$]: molecule A: Rh1–Cl1 2.4425(2), Rh1–P1 2.3075(2), Rh1–P2 2.3070(2), Rh1–B1 1.9767(9), Rh1–B2 2.0108(9), B1…B2 2.457(2), P1–Rh1–P2 176.025(9), B1–Rh1–Cl1 129.33(3), B2–Rh1–Cl1 154.58(3), B1–Rh1–B2 76.07(4), $\tau_{\text{B}1}$ 72.12(9), $\tau_{\text{B}2}$ 30.3(2); molecule B: Rh2–Cl2 2.4341(2), Rh2–P3 2.3030(2), Rh2–P4 2.3076(2), Rh2–B3 1.9884(9), Rh2–B4 1.9961(9), B3…B4 2.468(2), P3–Rh2–P4 176.344(9), B3–Rh2–Cl2 132.71(3), B4–Rh2–Cl2 150.74(3), B3–Rh2–B4 76.55(4), $\tau_{\text{B}2}$ 74.1(1), $\tau_{\text{B}4}$ 34.0(2).

The latter one, **2b**-**3b**, will exclusively be discussed, however, the geometrical data of **3b** do not differ significantly between both structures, as well as for the two independent molecules of **3b** within **2b**-**3b**. Whilst **3b** exhibits a different coordination geometry at the rhodium atom as **2b** and **4b**, a comparison with these complexes has to be done with due caution. The molecular geometry of **3b** may be deduced from the geometry of **2b** by removal of one PMe_3 ligand and subsequent reorganisation in the equatorial plane. Both the Rh–Cl and Rh–P distances decrease from **2b** to **3b**, the Rh–Cl distance by about 0.1 \AA , as no directly *trans* standing ligand is now present and the *trans*-P P–Rh distances, just significantly, by about 0.01–0.02 \AA . More informative are the changes within the equatorial plane. The

approximately linear angle B2–Rh1–Cl1 in **2b** is reduced by approx. 25° to 150–155°, whilst the B1–Rh1–Cl1 angle of 106.02(2)° in **2b**(PhMe) increases by the same amount to 129–133° in **3b**. The B–Rh–B angle does, consequently, not change significantly. The B…B distance however is in **3b** even smaller (by 0.1 Å) than in **2b**, as the B–Rh distances in **3b** is also reduced by about 0.1 Å. The fact that the B…B distance decreases upon reducing the coordination number under reorganisation of, essentially, only the equatorial plane implies that steric reasons are not essential for the small B…B distances in the six coordinated complexes **2b** and **4b**.

A comparison of the geometry of **3b** with other five coordinate rhodium(II) *bis*-boryl complexes, [Rh(PEt₃)₂(Cl)(Bcat)₂], [Rh(PPh₃)₂(Cl)(Bcat)₂], reported by Marder and co-workers and the complex [Rh(PPh₃)₂(Cl)(Bcat)(Bpin)] (only crystallographically characterised, see sections 1.a and 2.d) showed that the geometries are over all comparable. The acute B–Rh–B angle below 80° and a short B…B distance in the 2.5 Å range are found as common characteristics.^{S6}

In other words, for all *bis*-Bpin complexes short B…B distances (<2.6 Å) are observed, independently of the anionic (**2b**) or neutral auxiliary ligands (**4b**) or the coordination number (**3b**). Whereas for the *bis*-Bcat and BcatBpin complexes significantly longer B…B distances (>2.75 Å) are found in six coordinate complexes, whereas five-coordinate complexes show similarly short B…B distances.

2.d. $[\text{Rh}(\text{PPh}_3)_2(\text{Bcat})(\text{Bpin})(\text{Cl})](\text{CH}_2\text{Cl}_2)_{3.5}(\text{C}_5\text{H}_{12})_{0.6}$

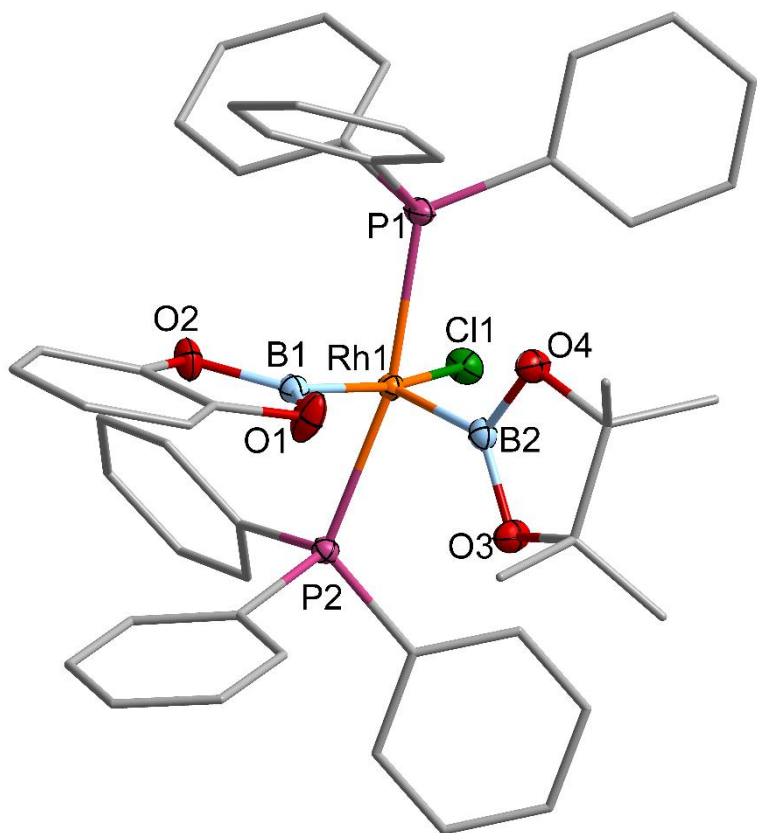


Figure S2d.1 Molecular structure of $[\text{Rh}(\text{PPh}_3)_2(\text{Bcat})(\text{Bpin})(\text{Cl})](\text{CH}_2\text{Cl}_2)_{3.5}(\text{C}_5\text{H}_{12})_{0.6}$. Selected distances (\AA) and angles ($^\circ$): Rh1–Cl1 2.4464(4), Rh1–P1 2.3190(4), Rh1–P2 2.3248(4), Rh1–B1 1.997(2), Rh1–B2 1.996(2), B1…B2 2.491(3), P1–Rh1–P2 167.30(2), B1–Rh1–Cl1 163.21(6), B2–Rh1–Cl1 119.59(5), B1–Rh1–B2 77.19(8), $\tau_{\text{B}1}$ 0.7(2), $\tau_{\text{B}1}$ 82.7(1).

2.e. $[\text{Rh}(\text{PMe}_3)_3(\text{Bcat})(\text{Bpin})(\text{L})]\text{[BArF]}$ ($\text{L} = \text{MeCN}$ (**5c**), MeNC (**6c**))

To elucidate the influence of different ligands *trans* to a boryl ligand we synthesised the complexes **5c** and **6c** (*vide supra*). The complexes crystallise in a monoclinic space group $P2_1/c$ as **5c** and as the solvate **6c**(THF) $_{0.53}$ (C₅H₁₂) $_{0.47}$ with one formula unit in the asymmetric unit.

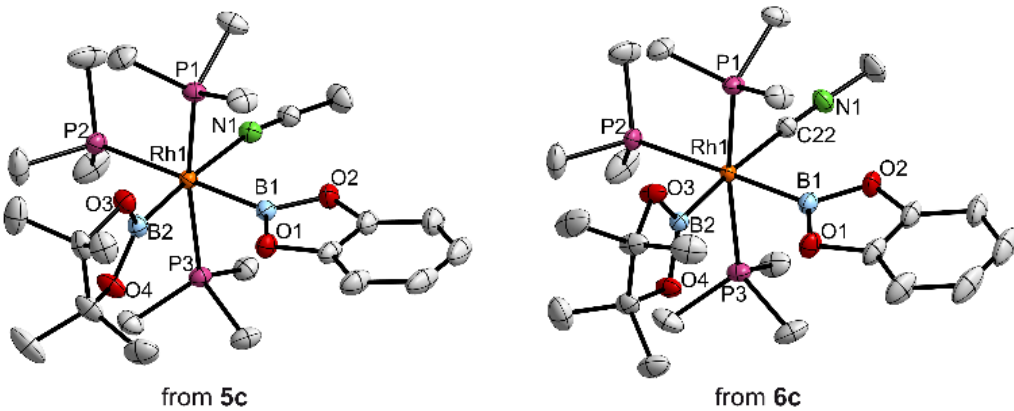


Figure S2e.1 Molecular structures of the cations in **5c** and **6c** from X-ray diffraction studies on **5c** and **6c**(THF) $_{0.53}$ (C₅H₁₂) $_{0.47}$. Selected geometrical data [Å / °]:

5c: Rh1–N1 2.209(2), Rh1–P1 2.3351(4), Rh1–P2 2.4115(4), Rh1–P3 2.3396(4), Rh1–B1 2.054(2), Rh1–B2 2.027(2), B1…B2 2.734(3), P1–Rh1–P2 166.57(2), B1–Rh1–P2 179.22(6), B2–Rh1–N1 175.49(7), B1–Rh1–B2 84.14(8), $\tau_{\text{B}1}$ 0.68(8), $\tau_{\text{B}2}$ 80.1(1).

6c: Rh1–C22 2.063(1), Rh1–P1 2.3369(4), Rh1–P2 2.3969(3), Rh1–P3 2.3367(3), Rh1–B1 2.056(1), Rh1–B2 2.080(1), B1…B2 2.755(2), P1–Rh1–P2 166.85(1), B1–Rh1–P2 177.74(5), B2–Rh1–C22 173.49(5), B1–Rh1–B2 83.51(6), $\tau_{\text{B}1}$ 5.99(6), $\tau_{\text{B}2}$ 82.22(6).

The structure of both complexes may be deduced from the structure of the chlorido complex **2c** by replacing the chlorido ligand with the neutral ligands acetonitrile or methylisonitrile, respectively (Figure 6).⁸ Structurally both complexes fit in the series **2c**, **5c**, **6c**, **4c**. While the general structure does not change significantly, the Rh1–B2 distances show the effect of the different *trans* ligand strengths being by about 0.05 Å shorter for the weak MeCN (**5c**) than for the stronger MeNC (**6c**) ligand. This increase is comparable to the change of 0.07 Å observed going from a chlorido ligand in **2c** to a phosphine ligand in **4c**.

3. References

- S1 N. C. Norman, A. G. Orpen, M. J. Quayle and E. G. Robins, *Acta Cryst.*, 2000, **C56**, 50–52.
- S2 D. Kratzert, J.J. Holstein and I. Krossing, *J. Appl. Cryst.*, 2015, **48**, 933–938.
- S3 D. Stalke, *Chem. Soc. Rev.*, 1998, **27**, 171–178.
- S4 O. V. Dolomanov, L. J. Bourhis, R. J. Gildea, J. A. K. Howard and, H. Puschmann, *J. Appl. Crystallogr.*, 2009, **42**, 339–34.
- S5 A. L. Spek, *Acta Cryst.*, 1990, **A46**, 194-201.
- S6 W. Clegg, F. J. Lawlor, T. B. Marder, P. Nguyen, N. C. Norman, A. G. Orpen, M. J. Quayle, C. R. Rice, E. G. Robins,A. J. Scott, F. E. S. Souza, G. Stringer and G. R. Whittell, *J. Chem. Soc., Dalton Trans.* **1998**, 301–310.